Master's thesis

NTNU
Norwegian University of Science and Technology
Faculty of Information Technology and Electrical Engineering
Department of Engineering Cybernetics

Eystein Gulbrandsen

# Model-Based Roasting Control

Master's thesis in Industrial Cybernetics
Supervisor: Morten Dinhoff Pedersen
May 2021

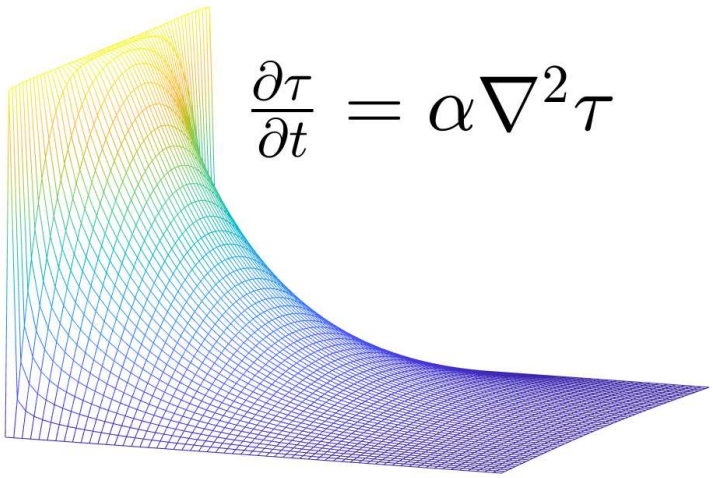


NTNU
Kunnskap for en bedre verden

Eystein Gulbrandsen

# Model-Based Roasting Control

Master's thesis in Industrial Cybernetics
Supervisor: Morten Dinhoff Pedersen
May 2021

Norwegian University of Science and Technology
Faculty of Information Technology and Electrical Engineering
Department of Engineering Cybernetics

NTNU
Kunnskap for en bedre verden

# Abstract

Cooking beef to perfection is an art. It can take many years of specialized training to achieve intuition for when the steak is perfectly done. Techniques such as fingertip methods or visual inspection are often deployed to assert if the steak is rare, medium or well-done. Research and comparison study shows that a combination of high initial temperature and prolong cooking time at a lower temperature are ideal for enhancing tenderness, juiciness, good colour and flavour. These studies also suggest that most households had a flawed estimation when the correct cooking temperature for meat occurred.

This thesis aims to investigate if the use of control theory may enhance the temperature profile in roasted meat. Such that optimal doneness might be attained. It is hypothesized that it can be hard to know when a steak is roasted to idealized doneness, even with a thermometer. The latent heat can make the steak overshoot or undershoot the desired doneness, which may be mitigated with a proper controller. We will assume one thermometer is used at the core of the roast, and the model can facilitate the rest of the unknown measurement of the temperature states.

In this thesis, a model predictive controller strategy was constructed with an analytical mathematical model. Based on the partial differential heat equation. This equation was first modelled in one dimension with two different approaches. The first model was based on a finite-difference approximation, and the second on a spectral method. Both the models were validated and simulated, and the spectral method was found most robust to be used with the model predictive controller.

The spectral method was extended into two-dimensional cylindrical coordinates and validated against an experiment. The experiment consisted of a round steak and tenderloin roasted in a domestic oven. They were equipped with thermal sensors, and the telemetry data was compared against a simulation of the two-dimensional spectral model. After tuning the thermophysical properties, the model and the telemetry data showed similar characteristic. Where the tenderloin sample performed best, it was concluded that the two-dimensional spectral model could facilitate the rest of the unknown measurement of the roast. Simulation of the model predictive controller resulted in an even temperature profile throughout the meat, with high heat applied at the start of the cooking process and gradually decreasing the input to steady-state temperature. The outcome of the simulations leads to the conclusion that using control theory can theoretically give idealized doneness.

# Sammendrag

Å tilberede biff til perfeksjon er en kunst. Det kan ta mange år med spesialisert trening for å oppnå intuisjon for når biffen er perfekt stekt. Teknikker som å klemme på biff med finger eller visuell inspeksjon blir ofte brukt for å hevde om biffen er rå, medium eller godt stekt. Forskning- og sammenligningsstudier viser at en kombinasjon av høy starttemperatur og forlenget steketid ved lavere temperatur er ideell for å få en biff med perfekt mørhet, saftighet, farge og smak. Disse studiene viser også at de fleste husholdninger hadde en feilaktig estimering på når riktig steketemperatur for kjøtt er nådd.

Denne oppgaven tar sikte på å undersøke om bruken av kontrollteori kan forbedre temperaturprofilen i stekt kjøtt, slik at optimalt stekeresultat kan oppnås. Det antas at det kan være vanskelig å vite når en biff er ferdigstekt til ønsket temperatur, selv med et termometer. Den latente varmen kan gjøre at biffen får høyere eller lavere enn den ønskede temperaturen, noe som kan korrigeres med en kontroller. Oppgaven bygger på at ett termometer brukes i kjernen av steken, og modellen kan kalkulere resten av de ukjente målingene av temperaturtilstandene.

I denne oppgaven ble en modellprediktiv kontrollerstrategi utviklet ved hjelp av en analytisk matematisk modell, basert på en partiell differensiell varmeligning. Denne ligningen ble først modellert i en dimensjon med to forskjellige metoder. Den første modellen var basert på en endelig forskjellsmetode og den andre på en spektralmetode. Begge modellene ble validert og simulert, og spektralmetoden ble funnet mest robust for å brukes med modellprediktiv regulering.

Den spektrale metoden ble utvidet til todimensjonale sylindriske koordinater og validert mot et eksperiment. Eksperimentet besto av en rundstek og indrefilet, stekt i en husholdningsovn. Biffene ble utstyrt med termiske sensorer, og telemetridataene ble sammenlignet med en simulering av den todimensjonale spektrale modellen. Etter eksperimentell tilpasning av de termofysiske egenskapene viste modellen og dataene lignende karakteristikk. Der indrefileten ga den mest optimale resultat, og det ble konkludert med at den todimensjonale spektralmodellen kunne finne rett temperatur i de øvrige områdene i biffen. Simulering av en modellprediktiv kontroller resulterte i en jevn temperaturprofil i hele kjøttet, med høy varme påført i begynnelsen av tilberedningsprosessen og gradvis redusert pådrag av tempeartur, til en stabil temperatur. Resultatet av simuleringene viser at kotrollteori kan anvendes til å gi et teoretisk og ideelt stekeresultat i en biff.

# Preface

This master thesis is the basis of the TTK4900 - Engineering Cybernetics and was conducted in the semester of 2021. The thesis concludes a two-year master degree program in Industrial Cybernetics at the Norwegian University of Science and Technology.

The project went through numerous phases to realise the outcome of interfacing the heat equation with a model predictive control—this resulted in a way to control a roast to a correct cooking temperature. It was engaging and had a steep learning rate. The author of this thesis had some previous experience with solving partial differential equations. Nevertheless, a realistic model poses more of a challenge.

The author of the thesis would describe himself as a hobby cook; however, he is not a food scientist nor a food engineer. Extensively litterateur search had to be filtered out. There are many opinions of what is seen as the correct internal temperature for different types of beef in the culinary arts. Therefore only a select few are examined in this thesis.

I want to give thanks to my supervisor Morten Dinhoff Pedersen. This thesis was made possible with his exceptional help and making his kitchen available for the experiment. I would also like to thank colleagues at NTNU, their support and insight. Finally, I would give my thanks to my family and my dog, who took me out on long walks and cleared my thoughts.

Eystein Gulbrandsen, Trondheim Mai 2021

# Nomenclature

| | |
|---|---|
| SLP | Sturm-Liouville Problem |
| SLE | Sturm-Liouville Equation |
| PID | Proportional Integral Derivative Controller |
| MPC | Model Predictive Control |
| PDE | Partial Differential Equation |
| ODE | Ordinary Differential Equation |
| BC | Boundary Condition |
| IC | Initial Condition |
| IBVP | Initial Boundary Value Problem |
| MIMO | Multiple-Input and Multiple-Output |
| MV | Manipulated Variables |
| OV | Output Variables |
| LTI | Linear Time Invariant |
| CVD | Chronic Vascular Diseases |
| IARC | International Agency for Research on Cancer |
| AAFC | Agriculture and Agri-Food Canada |
| WHO | World Health Organization |

# Contents

# List of Figures

# List of Tables

# 1 | Introduction

## 1.1 Background and Previous Work

There is a considerable amount of research and mainstream ways of cooking meat related to this work. This thesis will give a broad perspective on some of the research concerning temperature distribution while cooking meat. There are several perspectives in these adjacent research topics, the most notable being the relationship between temperature and cooking tender meat. Harold McGee, a leading author in the science of cooking, suggested that "*Cooking tender meat to perfection—so that its internal temperature is just what we want—is a real challenge*[1]". and the way to solve this is to use two-stage cooking with high heat applied first, followed by a prolonged lower cooking temperature.

Many culinary experts like to show how easy it is to cook a perfect steak with the right core temperature. However, research has demonstrated that this is not the case for most amateur cooks. Most amateurs' uses methods to determine cooked beef based on assumptions or pseudo information in media. Research shows that few uses thermometers and the thermometers used are less than reliable. Others use colour on the surface or skin as the only indicator. Only a tiny portion of the population uses several indicators to determine the right temperature, e.g. colour, internal temperature, the colour of meat juice, and the muscle's firmness. Known as the fingertip methods, which is not 100% reliable and can be an unsafe method, we must be aware that 1/3 of all food-based illnesses is related to undercooked meat. Undercooked meat may have an unsafe level of Salmonella and Campylobacter microbes.

This thesis aims to describe a methodology to cook a perfect steak, using cybernetics as a tool. Although considerable research has been devoted to modelling heat transfer and how it affect meat, less attention has been paid to using control theory to get an even temperature profile in meat. We propose that a model-based partial differential heat equation coupled with a model predictive controller could allow for perfectly roasted meat. The model predictive controller has been well-established in industrial application and has had a steady increase in different application over several decades [2]. It is used in various thermal applications; thermal power plants, the heat source in a household, heat exchanger [3, 4, 5] to mention few processes. The use of MPC in a household cooking process is sparsely investigated, and little information

on this topic was found in a literature search. Although MPC is commonly used in the food industry. E.g. optimizing food extruder, pasteurization and agriculture processes [6, 7, 8, 9].

## 1.2 Objective

This thesis aims to use the benefits of an MPC to reduce the possibility of overshooting/undershooting the temperature distribution in a roast. In order to implement this method, the effect of thermal energy, convective heat source and thermophysical properties needs to be integrated into the model. We can summarize the main objective as the following.

- Develop an analytical model based on the partial differential heat equations subjected to an initial boundary value problem and validate the model against empirical data.
- Implementing a Model Predictive Control strategy to achieve idealized doneness of a roast, considering the eating quality and thermal effect energy has on a steak.
- Discuss and describe the result and suggest future improvements to the model-based roasting controller.

## 1.3 Limitation

Limitation for this thesis:

- The MPC routine is not tested in a practical situation.
- Noise or disturbance are not accounted for in the MPC routine.
- Applicable for circular types of meat.
- Mass transport of fluids are not accounted for.
- Thermophysical properties are assumed not to vary in time.
- Heat flux is modelled with convective and radiative forcing. However, only convective is accounted for.

## 1.4 Structure of the Thesis

- **Chapter 2** - Presents theory into what a steak is composed of, how heat affects it, different types of cooking methods and how health and temperature in meat relates.
- **Chapter 3** - Will show how the one-dimensional heat equation can be derived and which types of thermophysical properties affect the model.
- **Chapter 4** - Gives a case study of modelling and solving the finite-difference approximations for the 1-D heat equation.
- **Chapter 5** - Presents an improved method to solve the 1-D heat equation with a spectral method.
- **Chapter 6** - Outline how an MPC can regulate the temperature in a roast and simulate the 1-D heat equation spectral method.
- **Chapter 7** - Derive the 2-D heat equation for a spectral method into cylindrical coordinates.
- **Chapter 8** - Covers the details of how the experiment is set up.
- **Chapter 9** - Shows the results and discuss the findings from the experiment and simulation of the MPC.
- **Chapter 10** - Presents the conclusion of this thesis.

# 2 Culinary Literature Research

## 2.1 Beef nutrition and composition

Meat contains approximately 75 % water, 19 % protein and 5 % fat. According to Food and Agriculture Organization, meat is defined as all parts of an animal intended for or is safe for human consumption [10].

One of the most important factors in a steak is marbling, which is the amount of fat streaking in a cut. Chefs want fat streaking in a steak. The most commonly referred top of the line example is the Kobe beef, which has fat spread evenly throughout the cut. The amount of fat streaking in beef and the age of the cattle is usually the common determinator to describe quality, e.g. a prime cut. However, as people also seek more healthy food with reduced risk of cancer and cardiovascular diseases, lean meat with little marbling is sought as preferred steaks [11]. The various parts of a cattle are usually divided into ribs, flank, shank, round steak and the top of the line parts sirloin and tenderloin. In the US, there is another part which seldom found in Norwegian cuts, a brisket. Briskets are usually barbequed over a long period because they are part of the front leg muscle, right above the shank [12]. Also, in Norway, farmers get a bonus for marbling and breeds like Charolais, Angus and Limousine [13]. Figure 2.1 and Figure 2.2 shows two different types of marbling.

Figure 2.1: Rib-eye steak: A steak with high marbling content

Figure 2.2: Striploin: A steak with lower marbling content

The beef sold is skeletal muscles, muscles that produce body movements. Some part of the meat is used to twitch the skin to keep flies away from the cattle; they are situated directly under the skin. The dominant structure of these muscles is fibres or bundles of fibres. These muscle fibres are long and thin. When a steak is cut, the cut seldom follows the whole length of the muscle fibre. When cattle are slaughtered, they are typically shackled and hung from their

back legs in a conveyer belt. The muscles in the rump region are stretched in this process, and the muscles in the front part of the cattle are usually free of constraints, and the muscles contracts as the cattle reach rigour. The stretched muscles show that the circular muscle fibres are far apart, but in the contracted muscles, they are close together. Meat with more circular muscle fibres, or transverse striations, tends to be tough. Therefore, the way the cattle hangs are related to the best part of the meat is in the rump regions, e.g. the loin cuts [14].

Meat is one of the most significant nutrients and energy-rich food product in most western households. It is considered necessary to maintain a healthy and balanced diet according to most nutrition recommendations. However, there are important health considerations since there is a relationship between cancer, metabolic disorders, cardiovascular diseases, and red meat. The nutritional composition in beef are grouped in [15]:

**Water**: Meat is a perishable food product, e.g. a food product with more than 60 % moisture. A larger amount of moisture means a reduction in shelf life, and that time changes the colour, odour, texture and flavour and composition of the meat. The amount of water is related to the type of nutrients the cattle get (for example, grass-fed cattle compared to corn fed cattle) and the animal's age. Younger animals are leaner and have a higher water content than older animals. Water content is usually 70 % in a steak, but younger animals have 72 % water content. Most of this water is bound in the muscle fibres, but some water is free and released while processing the meat. The holding abilities of the meat are changed when the muscle fibres get disrupt, for example, cut against the fibres, not along it or when grind, salt, or curing the meat.

**Carbohydrates**: The carbohydrates are stored in the liver and as glycogen in the muscle. Glycogen has an impact on the colour, texture, tenderness and water holding capacity of the steak. Glycogen is transformed into glucose and lactic acid when the cattle moves, ages or are in a stressful situation. When lactic acids increase, for example, during ageing, the pH lowers. The pH has a strong influence on muscle texture, tenderness, colour and water holding capacity. When the animal is stressed, i.e. just before slaughter, the pH rises, and as a result, the muscles gets dark, firm and dry due to depletion of glycogen reserves.

**Proteins and amino acids**: Meat is a protein-rich food source. In beef steaks, protein is 20-21 % depending on the cut. The highest protein source is chicken breast (34,5 %) and the lowest duck meat (12.3 %). The protein is also more digestible than most other protein-rich food sources, 92 % digestible amino acids compared to 57-71 % in beans and peas. Essential amino acids for a human body are the amino acids, e.g. the body's amino acids cannot produce themselves. Beef has a high content of 11 essential amino acids and seven non-essential amino acids (amino acids the body can produce).

**Fat**: Meat contains fatty tissues and is the energy deposits and protective padding in the skin and around organs as the heart and kidney. Fat is also

insulation, important for cattle that grace outdoors. Cooking has a significant effect on the fat, and during broiling and pan-frying, there is a significant loss in fat. Concerning health, the amount of cholesterol in the fat is of most importance: Beef has 62 mg/100 gram of meat than mutton 81 mg and pork 71 mg. Of the polyunsaturated fatty acids, Omega 3 is the most important from a health perspective. Seafood is the most important source of Omega 3, but meat can contribute to up to 20 % of the total intake of Omega 3.

**Minerals**: Macrominerals are minerals the body needs in larger amounts, and micro minerals are needed in small amounts. Beef is a primary mineral source for K, Cu, Fe, Zn and Mg and a minor source for Na and Ca.

**Vitamins**: Meat is a major source for the B complex vitamins riboflavin, thiamin, $B_6$ and $B_{12}$ [16].

## 2.2 Eating Quality

The quality of the steak is most commonly on the eating quality. Other factors customers bases their decision on the amount of visual fat and fat distribution in the steak, the colour of the meat, price, brand and cut of the steak [17].

### 2.2.1 Tenderness

Tenderness is a measurement of how easy we chew the steak. Juiciness is a measurement of the amount of meat juice released in the mouth while chewing. The beef flavour is measured on the cooked beef. The scale is 0-10 and measured by trained sensory panels [18].

Tenderness in beef is related to the type of cut, ageing treatment, and how the carcass is handled after butchering. The amount of collagen and the length of sarcomere fibres are the most important factors [19]. The sarcomere fibres are longer if they are stretched after butchering [20]. Stretching of the muscle to increase sarcomere length increases tenderness as much as 21 days of ageing [21]. Heat treatment to beef makes collagen tissue soluble; this results in tenderization of the beef [22].

A comparison of customer satisfaction of different cuts of meat from young bulls, heifers (young cow before birth) and steer (mature bulls) shows that the end temperature of the cooked beef is the most critical factors from a sensory perspective. Steak cooked at $55°C$ produced a tender and juicy steak compared to $74°C$. Tenderness correlates to juiciness, and beef flavour and tenderness increase when cooking the beef at a lower temperature over time. So, what is the best steak: Steers and heifers from Aberdeen Angus, Limousin and Charolais cooked to perfection at $55°C$ with an average tenderness of 5,1 (steers) – 5,2 (heifers) and juiciness 5,7 – 5,9 and beef flavour at 4,3 – 4,1 [18].

### 2.2.2 Cooking loss

Cooking loss is a reduction in water and soluble matters lost in the cooking process compared to raw meat. Cooking loss increases to temperature up to $70°C$. Cooking loss varies with different types of meat, for example, 31 % cooking loss in beef in an oven cooking at $200°C$ to 19 % cooking loss in beef in sous vide at $60°C$. Pan-frying of pork chops shows a marked increase in cooking loss over time: At $175°C$ for 75 seconds, the cooking loss is 11 %, but when doubling the frying time cooking loss increases to 25 % [23].

### 2.2.3 Maillard effect

The Maillard reaction is a chemical processed reached when frying meat. It is a chemical reaction between amino acids and reducing sugars that gives browned food its distinctive flavour. The effect happens at a temperature between $140°C$ and $160°C$, and at a higher temperature, caramelization is reached. Until the Maillard reaction occurs, the meat will have less flavour [23].

### 2.2.4 Resting time

Many chefs recommend resting time after the meat is cooked. The reason for this being that meat juices need to settle after cooking. In 2002 the Danish Meat Research Institute performed two tests: meat without resting time and steak eaten after 20 minutes resting time per the recommendation from the most popular cookbooks. The positive effects of resting was a more homogenous and well-done appearance in the steak. Overall, 20 minutes of resting time gave an average score ten % higher than the meat that had not rested. Concerning meat juices, the result showed little to no effect of the 20 minutes rest period than eating without a resting period. Resistance, meat flavour and tenderness were equal, whereas juiciness decreased for the steak that had rested 20 minutes compared to the steak eaten directly after cooking [24].

## 2.3 Effect of Thermal Energy on a Steak

Cooking meat is essential to achieve a safe and product that is palatable and easy to digest. The meat protein represents about 20 % of the weight of the beef, it represents the main part of the structure, and the protein undergoes substantial changes on heating and the quality of the beef. These changes are called denaturation, and the changes are directly related to tenderizing of the beef: slow cooking below $60°C$ activates the sarcoplasmic proteins (i.e. the proteins soluble in water) and fast heating up to $70 - 80°C$ deactivates these tenderizing proteins. One of these soluble proteins is myoglobin; the protein dissolved and gives a pink or red colour. During heating, myoglobin changes from pink to light tan colours. The activation process of sarcoplasmic proteins forms a gel of aggregated proteins glueing the meat fibres and fibre bundles together, creating an elastic and tender meat product. If the meat cuts are

from the front part of the beef, they need longer time to tenderize the beef than the stretched muscles on the hind part of the cattle.

The second major effect is the changes in connective tissues in the beef. The connective tissues are the tendons that connect the muscles to the bones. There are two primary connective tissues: The tough indigestible tendon fibres that wrap themselves around the muscles named silver skins and the collagen fibres. The silver skin toughens during heating, while the collagen dissolves between 65 - 67°$C$ into gelatin. This gel has good water holding capacity, while the collagen fibres dry out and become stiff. However, the meat seems tender due to the gelatin [25].

The third major effect is reduced water in the beef; studies show a reduction of 25-30 % water reduction. The water reduction accelerates between 60 – 80°$C$ due to shrinkage of tissues and muscle fibres in the steak, this forces water out of the steak. With increased temperature, more water is expelled. Tenderness in the steak increases substantially between 50 – 65°$C$ , and decreases from 65 – 80°$C$. The optimal correlation between increased tenderness and decreased juiciness is the optimal suggested cooking temperature for medium beef, 55 – 60°$C$ and 65 – 68°$C$ for pork [25].

The 4th effect is the change in fat. Fat content is related to the fat content in the beef subcutaneous (under the skin), intramuscular, and fast food used in the cooking process. Fat melts from 54 - 60°$C$ and is part of the fat loss in beef. However, we need to consider the effects of fat added to the cooking process: Compared to raw meat, traditional frying with 100 gram beef with a large amount of fat (75 gram of margarine) increased fat % in beef with 6 %. There were only be a slight difference in the frying time or resting time in the pan. The beef with the highest fat % lost fat during frying, while beef with low-fat % gained fat. The research concluded that the essential factor is fat % in raw meat, not the amount of fat used in frying. In total, the beef gained 0.5 % of fat during frying, but the beef with the most intramuscular fat reduced fat by 2.7 % [26].

### 2.3.1 Oven cooking

Cooking Methods has a great impact on the quality of meat, nutritional value as well as health. The heat in the household oven can rise to 250°$C$, and fluctuate the temperature. A rapid rise in oven temperature reduces total cooking loss in the meat [27]. The reduction in cooking loss is significant because high water capacity in the cooked meat is directly related to the tenderization of the meat [23]. Ovens with steam jet injection in the oven chamber reduces vapour from the meat and ensures a tender steak [28].

### 2.3.2 Frying

Frying is a process where meat, oil and heat creates water loss, intake of oil, spices etc., formation of crust, gelatinization of starch, aromatization, protein

denaturation and colour change via Maillard reactions, hydrolysis or oxidation, and oil polymerization [29].

### 2.3.3 Sous vide cooking

Sous vide cooking, or boil-in-bag, is a method of heating meat in a water bath at a precise temperature using a PID controller. The temperature in the water container is usually between 50 and 85 $°C$. The effect of sous vide is a longer cooking time than oven and frying, reduced damage to the proteins in the meat, which are temperature sensitive. Sous vide reduces cooking loss and preserves the water in the meat. Low temperature has a positive effect on the juiciness and tenderness of the beef [30].

## 2.4 Health and Temperature in Meat

Compared to the 1990s, cancer incidents in the population has increased with an average above 1% per year. Cancer is the most common reason for early death in Norway, with an incident of more than double compared to heart disease [31]. Nutrition explains between 30-70% of cancer, and a common denominator is heterocyclic amines in cooked beef. The amines occur when beef is cooked at a temperature above 150$°C$. Analysis shows a high concentration in fried, for example, barbequed meat, and 2-amino-1- methyl-6-phenylimidazo [4,5-b] pyridin (PhIP) is the heterocyclic amines most commonly found in beef. This amine creates colon, prostate cancer and breast cancer. Epidemiological studies show a clear correlation between increased consumption of red meat and increased prostate and colon cancer [32].

Other studies have revealed a clear correlation between intake of red meat and processed meat and chronic vascular diseases (CVD): Two and more meals every week with red meat or chicken increases CVD by 3-7 % [33]. A second factor is that processed meat, e.g. hamburgers, sausages etc., represents a higher risk of cancer than unprocessed meat. This is due to several factors, most notably the increased intake of salt, nitrate and nitrite and various other additives. These products end up in the digestive system as nitrosamine, and IARC (WHO's cancer research institute) has determined that this causes cancer [34].

A third factor is that undercooked meat, most notably undercooked chicken meat, explains $\frac{1}{3}$ of all foodborne illness outbreaks. In a study of European household's way of cooking chicken, researchers found out that the way most households determined correct cooking temperature was flawed. For example, the youngest group of participants considered skin colour as the best determinates of cooked chicken. However, lab tests showed undercooked meat and a high risk of catching Salmonella or Campylobacter microbes. Only a minority of the households used food thermometers. The study concluded that current practices in households do not reduce the pathogens to a safe level [35].

# 3 | Derivation of the One Dimensional Heat Equation

The problem to be understood in this thesis is to control a heat source such that a steak can get an optimized temperature profile. A temperature distribution problem can be model with a well-known Partial Differential Equation (PDE) known as the heat/diffusion equation. The PDE will propagate the temperature throughout the meat, with heated air/steam and radiative forcing on the protein boundary. For a given initial temperature. Therefore, must the temperature distribution adhere to both the temperature at the boundary and the initial temperature.

The physical derivation of the heat equation will be more apparent to understand if we start by looking at the one-dimensional heat equation with some underlying assumption. The slab of meat will be seen as uniform, with length $L$ and exposed to a thermal energy source. By adhering to the second law of thermodynamics, the thermal energy will be transferred from a section of higher heat to a section of less heat. The heat flow from one point to another in the solid. Will be governed by the physical principles of the law of heat conduction (a.k.a Fourier's law of heat transfer) and energy conservation.

## 3.1 Object

First, we will need to define the object: Let the internal heat of a region be enclosed in $\mathcal{D} \in \mathbb{R}^n$ with uniformed properties be exposed to a heat source. We denote a vector $\boldsymbol{x} = [x_1, \ldots, x_n]^T$ in $\mathbb{R}^n$ to be the spatial temperature at a given point $x_n$ at time $t$. The temperature distribution at point $x_n$ and time $t$ can be denoted by the function $\tau(x, t)$.

There will be assumed non-internal heat generation inside the region of the object nor dissipation of heat inside the region. Consequently, the heat source will only act on the boundary $\partial\mathcal{D}$. This can physically be described by assuming that the object is a rod, and surrounding the outside radial surface is an insulator. An insulator will ensure that no heat is transferred radially; only lateral heat transfer will occur along the rod. This means that only the endpoint of the rod will be exposed to the environment, i.e. the heat source. A rendition of this interpretation can be seen in Figure 3.1.

Since the thermal energy flows from a heat source into the region's boundary, the problem can be classified as a non-steady-state problem.

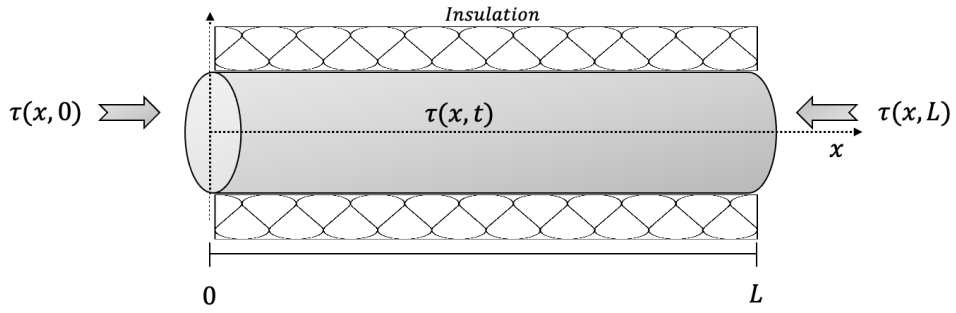


Figure 3.1: A visualization of the 1-D rod.

## 3.2 Derivation

We can relate the total amount of thermal energy inside the region of interest, $\mathcal{D}$. With the temperature, by integrating the heat over $\mathcal{D}$.

$$Q(t) = \int_{\mathcal{D}} \rho c_p \tau(x,t) dx \tag{3.1}$$

Where the specific heat capacity, $c_p$ and the density, $\rho$ of the material are set to a constant. We can describe the rate at which heat decreases in $\mathcal{D}$, and drop the dependency to make the notation more compact, viz.

$$\textit{"Time rate of heat decrees in } \mathcal{D}\textit{"} = \mathbf{q} = -\int_{\mathcal{D}} \rho c_p \frac{\partial \tau}{\partial x} dx \tag{3.2}$$

An empirical relationship known as Fourier's law of heat transfer states that: Heat tends to flow in the direction of decreasing temperature, and the rate of heat flow is proportional to the gradient of the temperature. Intuitively, we can observe that the velocity of heat flows faster if we have a larger temperature gradient and vice versa for lower temperature.

$$\mathbf{q} = -k \frac{\partial \tau}{\partial x} \tag{3.3}$$

Here, k is denoted as the thermal conductivity, and $\mathbf{q}$ is a heat flow vector field that will cross the surface $\mathcal{S}$ of the object. Or, in this case, since we are studying a one-dimensional case, the surface $\mathcal{S}$ are associated with the region's boundary $\partial\mathcal{D}$. An outward pointing normal vector, $\mathbf{n}$ is attached to the surface, and $d\mathcal{S}$ will be the surface measure over the boundary.

The quantity of $\mathbf{q}$ and $\mathbf{n}$ tells how much the heat flux is aligned with $\partial\mathcal{D}$. Lets define the following, $|\mathbf{q} \cdot \mathbf{n} \Delta A|$. Where $\Delta A$ is the cross-sectional area over $\partial\mathcal{D}$.

If $\mathbf{q} \cdot \mathbf{n} > 0$ thermal energy that are leaving $\partial\mathcal{D}$ and if $\mathbf{q} \cdot \mathbf{n} < 0$, thermal energy is entering the system.

Therefor we can express the total heat flow across the region, with a flux integral.

$$- k \int_{\partial\mathcal{D}} \frac{\partial \tau}{\partial x} \cdot \mathbf{n} \, d\mathcal{S} = \int_{\mathcal{D}} \mathbf{q} \cdot \mathbf{n} \, dx \tag{3.4}$$

By recalling the Divergence Theorem for a vector filed F.

$$\int_{\partial\mathcal{D}} F \cdot \mathbf{n} \, d\mathcal{S} = \int_{\mathcal{D}} \nabla \cdot F \, dx \tag{3.5}$$

We can insert Equation 3.4 in the Divergence Theorem and rewrite it as the following. Recognizing that $\nabla^2$ is the Laplacian of $\tau$, and a visualization can be seen Figure 3.2.

$$\text{"Total heat flow across } \partial\mathcal{D} \text{ "} = -k \int_{\partial\mathcal{D}} \frac{\partial \tau}{\partial x} \cdot \mathbf{n} \, d\mathcal{S} = -k \int_{\mathcal{D}} \nabla^2 \tau \, dx \tag{3.6}$$

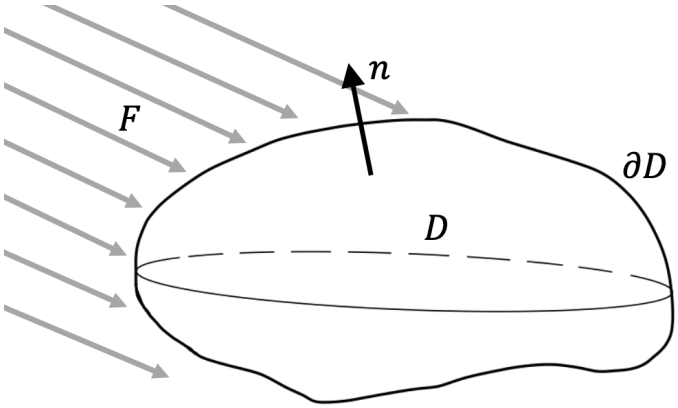


Figure 3.2: Heat flux $F$ that acts upon an arbitrary object.

Since we assumed that no heat is being generated nor lost inside the region. The only way in which heat can be dissipated or generated is if heat flows over the $\partial\mathcal{D}$. Hence the rate at which heat is decreeing/increase (Equation 3.2) and the total flow heat across the boundary (Equation 3.6) has to be equal viz.

$$\begin{aligned} &\int_{\mathcal{D}} \rho c_p \frac{\partial \tau}{\partial x} dx = k \int_{\mathcal{D}} \frac{\partial^2 \tau}{\partial x^2} \, dx \\ \Leftrightarrow &\int_{\mathcal{D}} \left( \rho c_p \frac{\partial \tau}{\partial x} - k \frac{\partial^2 \tau}{\partial x^2} \tau \right) dx = 0 \end{aligned} \tag{3.7}$$

In order for the Equation 3.7 to hold for an arbitrary $\mathcal{D}$, the integrand has to be zero. Thus, we can write out the one-dimensional partial differential heat equation as seen in Equation 3.8. Which states that the partial derivative of temperature to time is proportional to the second partial derivative to space. Intuitively, this entails that when the temperature distribution at a given point curve. The temperature tends to change in the curvatures' direction. How fast the temperature changes is dependent on the magnitude and sign of the curvatures.

$$\frac{\partial \tau}{\partial t}(x,t) = \frac{k}{\rho c_p}\frac{\partial^2 \tau}{\partial x^2}(x,t), \qquad for \quad 0 \leq x \leq L, \quad t \geq 0 \tag{3.8}$$

Here the $k$ is the thermal conductivity, $\rho$ density and $c_p$ heat capacity. These units can be group into a constant, denoted the thermal diffusivity.

$$\alpha \triangleq \frac{k}{\rho c_p} \tag{3.9}$$

## 3.3 Boundary Conditions and Initial Condition

The Heat Equation requires two additional pieces of information to give a unique solution, the Initial Condition (IC) and the Boundary Conditions (BC). The IC will describe the temperature distribution for the object at $\tau(x,0)$, and the BC will impose the specific values for the solution on $\partial\mathcal{D}$. For the one-dimensional case the thermal energy will act on $\tau(0,t)$ and $\tau(L,t)$.

Since the boundary interacts with the environment, we need to see how heat flux acts upon the endpoint of the object. One way of doing this is to study Newton's law of cooling, which specifies that heat transfer is proportional to the difference between the surrounding environment and the material. For the one-dimensional case, we can write it as the following.

$$\begin{aligned} q_0 &= hA\left(u(t) - \tau_0\right) \\ q_L &= hA\left(u(t) - \tau_L\right) \end{aligned} \tag{3.10}$$

Here, $u(t)$ is the heat source (environmental temperature) acting upon the object, $A$ is the area (obviously for the 1-D case $A = 1$), and $h$ is the heat transfer coefficient.

Fourier's law for two boundaries may be written as.

$$\begin{aligned} q_0 &= -k\left(\frac{\partial \tau}{\partial x}\right)_0 \\ q_L &= -k\left(\frac{\partial \tau}{\partial x}\right)_L \end{aligned} \tag{3.11}$$

By combining Equation 3.10 with Equation 3.11, the interface from Newton's law of cooling can relate the heat flux from Fourier's law at the boundary of the object. We have then derived an expression for the boundary conditions for the heat equation, known as the Robin boundary condition viz.

$$q_{\{0,L\}} = h\left(u(t) - \tau_{\{0,L\}}\right) = -k\left(\frac{\partial \tau}{\partial x}\right)_{\{0,L\}} \tag{3.12}$$

We can look at three special cases, known as the Dirichlet boundary condition, Neumann boundary condition and Robin boundary condition.

**Dirichlet boundary condition:**

Suppose $k \ll h \to \frac{k}{h} \sim 0$, the BC then becomes.

$$\begin{aligned} u(t) - \tau_{\{0,L\}} &= -\frac{k}{h}\left(\frac{\partial \tau}{\partial x}\right)_{\{0,L\}} = 0 \\ \Rightarrow u(t) &= \tau_{\{0,L\}} \end{aligned} \tag{3.13}$$

Which can be seen as a fixed temperature boundary condition.

**Neumann boundary condition:**

If we look at the other case of $h \ll k \to \frac{h}{k} \sim 0$, the BC then becomes.

$$\begin{aligned} -\left(\frac{\partial \tau}{\partial x}\right)_{\{0,L\}} &= \frac{h}{k}\left(u(t) - \tau_{\{0,L\}}\right) = 0 \\ \Rightarrow \left(\frac{\partial \tau}{\partial x}\right)_{\{0,L\}} &= 0 \end{aligned} \tag{3.14}$$

This then become a zero flux boundary condition and is a fully insulated system, where no heat flux is exchanged at the boundary.

**Robin boundary condition:**

The general case can be seen as a mixed case of both the previous BC. Whereas both $h$ and $k$ comes into play. It can be noted that this is a linear expression of the Dirichlet and Neumann boundary conditions and are homogeneous if $u(t) = 0$.

$$\begin{aligned} -k\left(\frac{\partial \tau}{\partial x}\right)_0 &= h\left(u(t) - \tau_0\right) \\ k\left(\frac{\partial \tau}{\partial x}\right)_L &= h\left(u(t) - \tau_L\right) \end{aligned} \tag{3.15}$$

Summarized, the Initial Boundary Value Problem (IBVP) for the homogeneous PDE on an arbitrary interval $x \in \mathcal{I} \to \mathbb{R}$ becomes.

$$\begin{array}{lll} \text{PDE:} & \tau_t(x,t) = \alpha\nabla^2\tau(x,t) & x \in \mathcal{I}, t > 0 \\ \text{IC:} & \tau(x,0) = f(x) & x \in \mathcal{I} \\ \text{Dirichlet BC:} & \tau(0,t) = \tau(L,t) = u(t) & \\ \text{Neumann BC:} & \tau_x(0,t) = \tau_x(L,t) = 0 & \\ \text{Robin BC:} & a_0\tau_x(0,t) - a_1\tau(0,t) = 0 & \\ & a_3\tau_x(L,t) + a_4\tau(L,t) = 0 & \end{array} \tag{3.16}$$

## 3.4 Maximum Principle

We asserted that the heat can only enter or dissipate through the boundary point. Logically this entails that the maximum or minimum heat for the system is found at the boundaries or if the temperature distribution at $\tau(x,0) \geq \tau(x,t)$. This can be asserted through the maximum principle.

**Theorem 3.4.1** ***Maximum principle****: Suppose $\tau(x,t)$ solves the heat equation in a finite space time rectangle, $R$, in the domain $0 \leq x \leq L$, $0 \leq t \leq T$. Then the maximum values for $\tau(x,t)$ is assumed to either be at the initial value of $\tau(x,0)$ or on the boundary's, i.e. $\tau(0,t)$ or $\tau(L,t)$. Let a set be denoted by $\Omega = \{(x,t) \in R \mid t = 0 \vee x = 0 \vee x = L\}$. Then the maximum principle is on the form*

$$\max_{(x,t)\in R}\{\tau(x,t)\} \leq \max_{(x,t)\in\Omega}\{\tau(x,t)\} \tag{3.17}$$

***Remark:*** *A maximum also suggests that a minimum can be found, viz* $\min\{\tau(x,t)\} = -\max\{\tau(x,t)\}$.

**Proof:** Suppose $\tau$ is a solution that satisfies the heat equation $\tau_t - \alpha\nabla^2\tau = 0$. Let an arbitrary interior point be defined by $(x_0,t_0)$ and $\tau$ be perturbed by a small positive value such that $v = \tau + \epsilon x^2$, viz.

$$\begin{aligned} v_t - \alpha\nabla^2 v &= \tau_t - \alpha\nabla^2\tau - 2\alpha\epsilon \\ \Rightarrow v_t - \alpha\nabla^2 v &= -2\alpha\epsilon < 0 \end{aligned} \tag{3.18}$$

By contradiction we can see that, if the maximum value occur inside the interior $(x_0,t_0) \in R \notin \Omega$. The laplacian has to be $-\alpha\nabla^2 v \geq 0$, and the inequality will not be satisfied.

$$0 \leq -\alpha\nabla^2 v = -2\alpha\epsilon < 0 \tag{3.19}$$

Then the maximum values for $v$ must therefore occur at the boundary, $\Omega$.

$$v(x,t) \leq \max_{(x,t)\in\Omega}\{v(x,t)\} \tag{3.20}$$

Similarly, for the solution $\tau$, we can show.

$$\begin{aligned} \tau(x,t) + \epsilon x^2 &\leq \max_{(x,t)\in\Omega} \{\tau(x,t) + \epsilon L^2\} \\ \Rightarrow \tau &\leq \max_{(x,t)\in\Omega} \{\tau(x,t) + \epsilon(L^2 - x^2)\} \end{aligned} \tag{3.21}$$

Then taking the limit of $\epsilon \to 0_+$

$$\tau(x,t) \leq \max_{(x,t)\in\Omega} \{\tau(x,t)\} \tag{3.22}$$

Thus, the maximum value must be in the closed set of $\Omega$. $\square$

## 3.5 Thermophysical Properties

The thermophysical properties of the meat govern the thermal dynamics of the heat equations. These properties are needed to estimate the time it takes to heat or chill the object. Since the thermal properties are dependent on which direction the muscle grains is to the heat flux, chemical composition and temperature. Can the properties be calculated with mass fractions of water, protein, fat and carbohydrate contents [36] or with the heat equation. Alternatively, the thermal properties can be found by direct empirical studies. Agriculture and Agri-Food Canada(AAFC) is an example of an organization that conduct theses type of studies [37].

### 3.5.1 Internal Thermophysical Properties

The thermal diffusivity is defined by the heat capacity, density and thermal conductivity of an object. All of these constants have transient and temporal properties for different types of cuts. The thermal diffusivity is an important constant for modelling the heat equation; it is a measure of how the thermal dynamics/concavity is shaped. This implies that a large value would give a steep gradient, and a low value would soften the gradient. In other words, it can be seen as the thermal inertia of an object. Although, lookup tables for isotropic materials such as steel, copper, and other commonly study isotropic materials are readily available. Are the thermal diffusivity constant of meat scarcely investigated [38].

The thermal diffusivity and thermal conductivity will be considered for a round beef, tenderloin and ham. The three types of meat have similar composition of water, fat and protein and are therefore chosen. They will be estimated with a linearized function, and composition data from the book *ASHRAE Handbook: Refrigeration American Society of Heating, Refrigerating and Air-Conditioning Engineers*. The thermophysical properties are given in a domain of $\tau \in [-40, 140]$. Since the temperature for food is often considered for storage, such as freezing and preventing foodborne illnesses. The *ASHRAE handbook* book notes that " *In general, thermophysical properties of a food or beverage are well behaved when its temperature is above its initial freezing point* "[38].

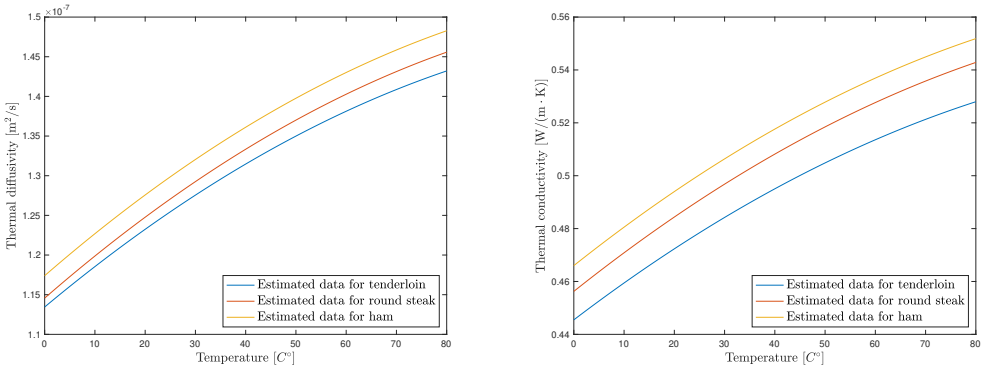


(a) $\alpha$: Thermal diffusivity. (b) $k$: Thermal conductivity.

Figure 3.3: Estimation of thermophysical properties for $\tau \in [0, 80]$.

An empirical study conducted by the AAFC. Found that thermal conductivities of four types of meat increased nearly linearly, for particles based foods in the temperature range $20 - 60°C$ and started to stabilized after $60 - 80°C$. The thermal diffusivity in the study was calculated based on density, thermal conductivity, and specific heat observed under the experiment [37], and can be seen in Figure 3.4.

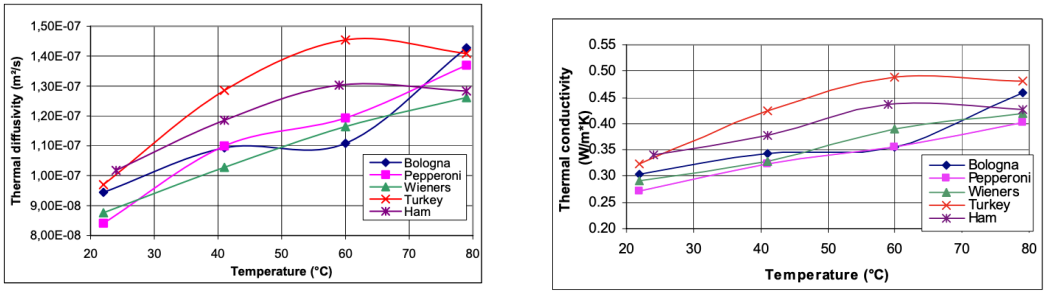


(a) $\alpha$: Thermal diffusivity. (b) $k$: Thermal conductivity.

Figure 3.4: An empirical study of different thermophysical properties [37].

### 3.5.2 External Thermophysical Properties

**The heat transfer coefficient:**

Is the proportional constant used in Newton's law of cooling and is an interface between a heat source and the material. It describes how the convective of a heated/cooled fluid flows over the material based on the body's geometry. Note that convection only appears for fluids, not inside a solid.

$$Q = h \cdot A \cdot (T(t) - T_{\text{env}}) \tag{3.23}$$

An easy way to interpret how the coefficient affects an object is to think about what occurs if that object is exposed to water and air. Water has a larger value of heat transfer capacity compared to stationary air. As $h$ increase, the

rate of heat transfer is faster out of the object. Analogous to being on land and plunging into the water.

Two types of convection can take place; natural convection and forced convection. Natural convection occurs from density difference in fluid, perturbed by a thermal energy source, which induces a motion to the fluids. Forced convection is fluid in motion from a fan or similar devices, which forces heat/chilled fluid over the object. The heat transfer coefficient will be affected by which type of convection is taking place.

J. Cernela et al. investigated the heat transfer for a domestic oven and noted that studies are often aimed towards industrial application and sparsely investigated in a domestic apparatus. The study found that the domestic oven gave a heat transfer coefficient of 6 $W/m^2C$ to 16 $[W/m^2C]$ under free and forced convection [39]. The article study only one type of domestic oven, and the result may vary for different types of oven. From the paper of A, Kondjoyan et al., an aluminium sample was subject to different fluids to assert the heat transfer coefficient in a domestic oven. Figure 3.5 shows the findings.

| Cooking or cooling systems | | Conditions | h ($Wm^{-2}$ $K^{-1}$) |
|---|---|---|---|
| Water bath | Stirred | 95 °C | 2174 ± 174 |
| | Non-stirred | 50 °C | 821 ± 90 |
| | Non-stirred | 70 °C | 962 ± 98 |
| | Non-stirred | 90 °C | 1190 ± 101 |
| | Non-stirred ice-water | ≈0 °C | 374 ± 10 |
| Air cooling, free convection | Ambient/room temperature | 20 °C | 6.5 ± 1 |
| Fan-assisted oven | Dry air | 100 °C | 51 ± 5 |
| | 10% steam injection | 100 °C | 134 ± 13 |
| | steam | 100 °C | 291 ± 29 |

Figure 3.5: A table of different heat transfer coefficient [40].

**Biot number:**

It can be helpful to work with a dimensionless quantity when studying a heat transfer problem. The Biot number relates the internal conductive resistance in the body with external convention resistance at the body's surface and can accordingly be defined.

$$\text{Bi} \triangleq \frac{h}{k} L_c \qquad \textit{Where, } L_c = \frac{V_{body}}{A_{surface}} \tag{3.24}$$

From section 3.3 we establish that the Robin condition was a linear expression of Dirichlet and Neumann conditions. We can observe that for a high value of the Biot number, i.e. $h \gg k$. The internal conductive resistances within the object is high, and the boundary condition reduces to the Dirichlet boundary conditions. For the case of a low Biot number, i.e. $h \ll k$. The external conductive resistances at the object's surface are high and reduces to the Neumann boundary conditions. Values for the Biot numbers are often categorised by.

$$\begin{cases} \text{Bi} > 40 & \text{External resistance is negligible} \\ \text{Bi} < 0.1 & \text{Internal resistance is negligible} \\ 0.1 \leq \text{Bi} \leq 40 & \text{Mix-case of external and internal resistance} \end{cases} \tag{3.25}$$

# 4 Finite-Difference Approximations for the 1-D Heat Equation

The main goal for this chapter is to observe the temperature evolution over time with a numerical solution to the 1-D heat equation. This implies that the heat equation needs to be solved, given the initial temperature distribution and boundary conditions that satisfy the PDE. We start by looking at a numerical approach for the solution.

## 4.1 Modeling

The one-dimensional heat equation will be considered for $\tau : [0, L] \times [0, \infty) \to \mathbb{R}$ for a given temperature point $x$ at time $t$. It can be noted that we are working with a numerical solution to the heat equation and can only find a solution for a finite time $t_{max}$.

$$\frac{\partial \tau}{\partial t} = \alpha \frac{\partial^2 \tau}{\partial x^2} \tag{4.1}$$

The solution of the heat equation has to adhere to the boundary condition and the initial conditions. Let the end and start point, plus a small distance $\epsilon$, be set equal to the temperature from the heat source, $u(t)$. Such that the Dirichlet conditions govern the boundary condition. Let the initial temperature distribution be assumed constant.

$$\begin{aligned} &\text{IC:} && \tau(x, 0) = T_0 \\ &\text{BC:} && \tau(0, t) = T^n_{i=0-\epsilon} = u \\ & && \tau(L, t) = T^n_{i=L+\epsilon} = u \end{aligned} \tag{4.2}$$

## 4.2 Numerical Solution

In order to find a numerical solution to the 1-D Heat Equation, a grid is constructed with $n \times i$ points. Temperature is approximated at a given grid

point, with a spatial step size in the $x$-direction and a time-step in the $t$-direction. An illustration of this can be seen in Figure 4.1.

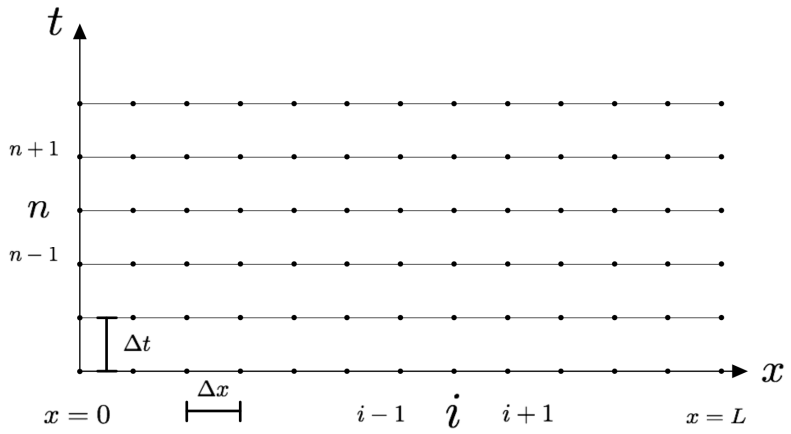


Figure 4.1: A Mesh used for the solution to the one-dimensional heat equation.

The right side of the continuous derivatives from Equation 4.1 can be approximate with the second-order central difference approximation. Let the grid point of $T(x_{i+1})$ and $T(x_{i-1})$ be a approximated by the Taylor series, viz.

$$T_{i+1} = T_i + \Delta x \frac{\partial T}{\partial x}\bigg|_{x_i} + \frac{\Delta x^2}{2}\frac{\partial^2 T}{\partial x^2}\bigg|_{x_i} + \frac{(\Delta x)^3}{3!}\frac{\partial^3 T}{\partial x^3}\bigg|_{x_i} + \cdots \tag{4.3}$$

$$T_{i-1} = T_i - \Delta x \frac{\partial T}{\partial x}\bigg|_{x_i} + \frac{\Delta x^2}{2}\frac{\partial^2 T}{\partial x^2}\bigg|_{x_i} - \frac{(\Delta x)^3}{3!}\frac{\partial^3 T}{\partial x^3}\bigg|_{x_i} + \cdots \tag{4.4}$$

A second order central difference of point $T(x_i)$ can be found by the summation of the neighbors grid point, i.e. grid point of $T(x_{i+1})$ and $T(x_{i-1})$.

$$T_{i+1} + T_{i-1} = 2T_i + (\Delta x)^2 \frac{\partial^2 T}{\partial x^2}\bigg|_{x_i} + \frac{2(\Delta x)^4}{4!}\frac{\partial^4 T}{\partial x^4}\bigg|_{x_i} + \cdots \tag{4.5}$$

Solving for the second partial derivative, and group the higher-order polynomial into the big O-notation yields.

$$\frac{\partial^2 T}{\partial x^2}\bigg|_{x_i} = \frac{T_{i+1} - 2T_i + T_{i+1}}{\Delta x^2} + \mathcal{O}\left(\Delta x^2\right) \tag{4.6}$$

Thus, one can combine Equation 4.1 with Equation 4.6, dropping the big O-notation to Equation 4.7. Denoting a new constant $b$, that holds the thermal diffusivity constant divided by the step length squared.

$$\frac{\partial T_i^n}{\partial t} = b\left(T_{i+1}^n - 2T_i^n + T_{i-1}^n\right) \qquad , b \triangleq \frac{\alpha}{\Delta x^2} \tag{4.7}$$

A state-space representation is formulated on the form of Equation 4.8.

$$\begin{aligned}\dot{\mathbf{x}}(x,t) &= \mathbf{A}\mathbf{x}(x,t) + \mathbf{B}\mathbf{u}(t)\\ \mathbf{y}(x,t) &= \mathbf{C}\mathbf{x}(x,t) + \mathbf{D}\mathbf{u}(t)\end{aligned} \tag{4.8}$$

Thus, it is possible to represent Equation 4.7 as seen in Equation 4.9. Where the $T_i$ is on the diagonal of the $\mathbf{A}$ matrix, and the $T_{i+1}$, $T_{i-1}$ is on the sub and super diagonal respectively [1]. In addition, it should be noted that the boundary condition from Equation 4.2 will make up the controller input, $\mathbf{B}$, for the state space model. I.e. $u_{i,1} = T^n_{i=0-\epsilon}$ and $u_{i,2} = T^n_{i=L+\epsilon}$, where $\epsilon$ is a small distance outside the region of interest.

$$\dot{\mathbf{x}}(x,t) = \begin{bmatrix} -2b & b & 0 & \dots & 0 \\ b & -2b & b & & \vdots \\ 0 & b & -2b & & 0 \\ \vdots & & & \ddots & b \\ 0 & \dots & 0 & b & -2b \end{bmatrix} \begin{bmatrix} T^n_0 \\ T^n_1 \\ \vdots \\ T^n_i \\ \vdots \\ T^n_L \end{bmatrix} + \begin{bmatrix} b & 0 \\ 0 & 0 \\ \vdots & \vdots \\ 0 & 0 \\ 0 & b \end{bmatrix} \begin{bmatrix} u_{i,1} \\ u_{i,2} \end{bmatrix} \tag{4.9}$$

The temperature of the object can be measured at a given grid point $i$ with the $\mathbf{C}$ matrix. Measurements taken between two grid points can also be done via interpolation. In addition, we assume that there is no direct feedthrough, $\mathbf{D} = 0$.

## 4.3 Discretization of the 1-D Heat Equation

By recognizing Equation 4.10 as an analytical solution for a continuous state-space model. An exact discretization of the state-space representation is formulated in Equation 4.11. Under the condition that the controller input stays constant for each time-step and are piecewise smooth $T : t = kT$. I.e. $\mathbf{u}[k] \simeq \mathbf{u}(t), kT \leq t < (k+1)T$.

$$\mathbf{x}(t) = e^{\mathbf{A}t}\mathbf{x}(0) + \int_0^t e^{\mathbf{A}(t-\nu)}\mathbf{B}\mathbf{u}(\nu)d\nu \tag{4.10}$$

$$\begin{aligned}\mathbf{x}[k+1] &= e^{\mathbf{A}T}\mathbf{x}[k] + \left(\int_{kT}^{(k+1)T} e^{\mathbf{A}[(k+1)T-\nu]}d\nu\right)\mathbf{B}\mathbf{u}[k]\\ &= e^{\mathbf{A}T}\mathbf{x}[k] + \left(\int_0^T e^{\mathbf{A}v}dv\right)\mathbf{B}\mathbf{u}[k]\\ &= e^{\mathbf{A}T}\mathbf{x}[k] + \mathbf{A}^{-1}\left(e^{\mathbf{A}T} - \mathbf{I}\right)\mathbf{B}\mathbf{u}[k]\end{aligned} \tag{4.11}$$

[1] Also know as the Toeplitz matrix

Where,

$$v(\nu) \triangleq (k+1)T - \nu, \quad d\nu = -dv \tag{4.12}$$

This yields an exact discretization for the state-space model of the one-dimensional heat equation.

$$\begin{aligned} \mathbf{x}[k+1] &= \overbrace{e^{\mathbf{A}T}}^{\mathbf{A_d}} \mathbf{x}[k] + \overbrace{\left(\mathbf{A}^{-1}\left(e^{\mathbf{A}T} - \mathbf{I}\right)\right)\mathbf{B}}^{\mathbf{B}_d} \mathbf{u}[k] \\ \mathbf{y}[k] &= \underbrace{\mathbf{C}}_{\mathbf{C}_d} \mathbf{x}[k] \end{aligned} \tag{4.13}$$

# 4.4 Preliminary simulation validation for an edge case

The preliminary simulation for the numerical solution of the 1-D heat equation are simulated in Matlab, and the simulation parameters consist of the following:

| Symbol | Variable | Value | Unit |
|---|---|---|---|
| L | Length | 5 | $[cm]$ |
| $\alpha$ | Thermal diffusivity | $1.3e-7$ | $[m^2/s]$ |
| $T_0$ | Initial/-Room Temperature | 20 | $[^\circ C]$ |
| $T_{cutoff}$ | Internal core temperature | 65 | $[^\circ C]$ |

Table 4.1: Parameter values for the preliminary simulation of the finite difference approximation of the heat equation.

The step function for the simulated heat source.

$$u(t) = \begin{cases} 200 & \text{if } \tau(L/2,t) \leq T_{cutoff} \\ 20 & \text{if } \tau(L/2,t) > T_{cutoff} \end{cases} \tag{4.14}$$

Before introducing a controller for regulating the heat source, we will simulate what occurs if a rod of simulated meat is exposed to a constant heat source. The simulated meat is removed from the heat source when the core temperature reaches $T_{cutoff}$, and the room will act as a heat sink. Furthermore, the heat source/sink will have a sizeable impact on the boundary of the solution. We can test if the finite-difference approximation can handle a stiff problem for some of the solution's stencil components.

Figure 4.2b shows how the temperature propagates through the meat over 50 minutes. We can observe that the temperature changes quite aggressively at the boundary, which make the solution stiff. This seems logical; since heat flux can only enter through the object's boundary, and convection has not been considered. Therefore, it can be seen as a fixed temperature boundary condition.

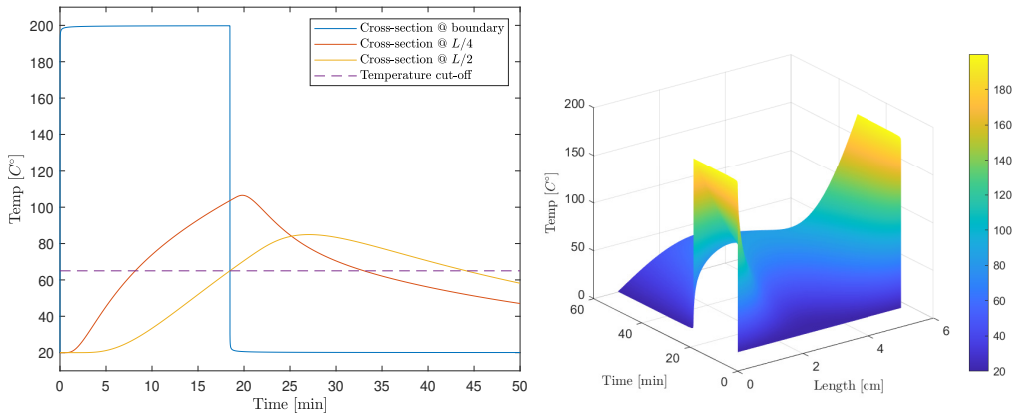


(a) A 2-d plot of three cross-sections.

(b) A 3-d Plot of the simulation.

Figure 4.2: A simulation of a rod of meat, done with the finite-difference approximation

Since the heat equation describes how temperature is distributed, at a given point, $x_i$. It will curve proportionally to the nearest neighbour's stencil. We can observe that the temperature changes with the magnitude and sign of the direction of the curvature. The heat source, $u(t)$, alters the temperature of the object's interior—both in a positive and negative gradient. This can particularly be seen in Figure 4.2b where the boundary has high curvature relative to its nearest neighbours, i.e. the heat source. Further inside the region of the object, the curvature is less predominated due to a less intensive gradient of the neighbours. By this logic, we can see that the material has a more prolonged time to gain and dissipate thermal energy the closer we get to the object's core.

From Figure 4.2a we can observe that the object reach an internal temperature of $T = 65°C$ at $t \approx 18$ $[min]$, and are then exposed to the room temperature. Even though the temperature at the boundary rapidly decreases, the residual heat from the region surrounding the core. Will still heat up the core of the object. This can be mitigated by taking the meat out at a lower temperature than the idealized core temperature and let the residual heat diffuse through to the right internal temperature. However, this will fast be subject to guessing at which time it should be taken out. As we further develop the model, we will introduce an optimized controller, MPC. Which gives optimal controller sequences to optimize the temperature distribution of the meat. This will remove the notion of when and how long the meat has to be exposed to the heat source and when it can be removed from the heat source.

### 4.4.1 Validation Error

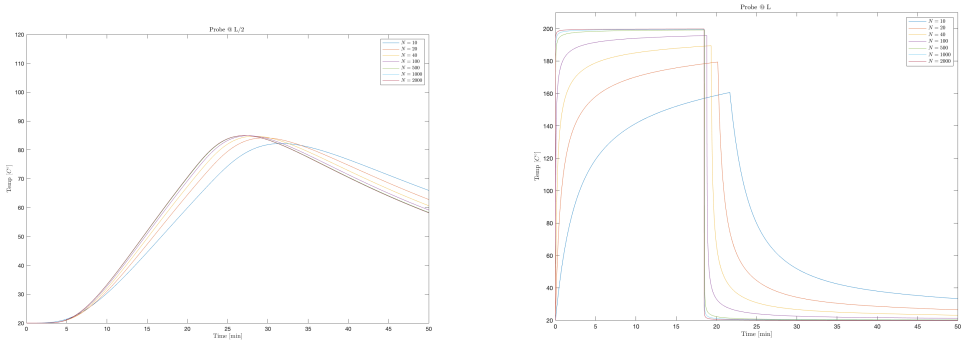

(a) The probe is at half the length of the meat.

(b) The probe is at the boundary of the meat.

Figure 4.3: A plot to showcase different resolution of the grid size

The second-order finite-difference method is a local method of approximating the spatial temperature using the two nearest neighbours. It has a truncation error of $\mathcal{O}(\Delta x^2)$, i.e. the error decreases quadratically for a larger grid size. This yields a good approximation for a non-stiff problem since the curvature can be seen as a polynomial approximation of the stencil. This can be seen in Figure 4.3a. Whereas increasing the number of grid size, the curvature of the plot is almost identical. However, when we introduce a high heat source at the boundary, the PDE becomes stiff and can increase/decrease exponentially. Figure 4.3b shows that for a non locally polynomial approximation the truncation error of $\mathcal{O}(\Delta x^2)$ is not sufficient enough (for $N < 500$). Yielding a poorer estimate of the stiff part of the solution and alters the dynamics of the model. We can keep increasing the grid size in order to satisfy an acceptable approximation of the stiff part. However, this comes at the cost of being computationally expensive and the exact discretization may be unmanageable. From the heavy matrix exponential and the inverse operation of the system matrix, $\mathbf{A}$. Especially if we were to rephrase the Toeplitz matrix to a higher-dimensional case or use other schems, i.e. Crank–Nicolson method.

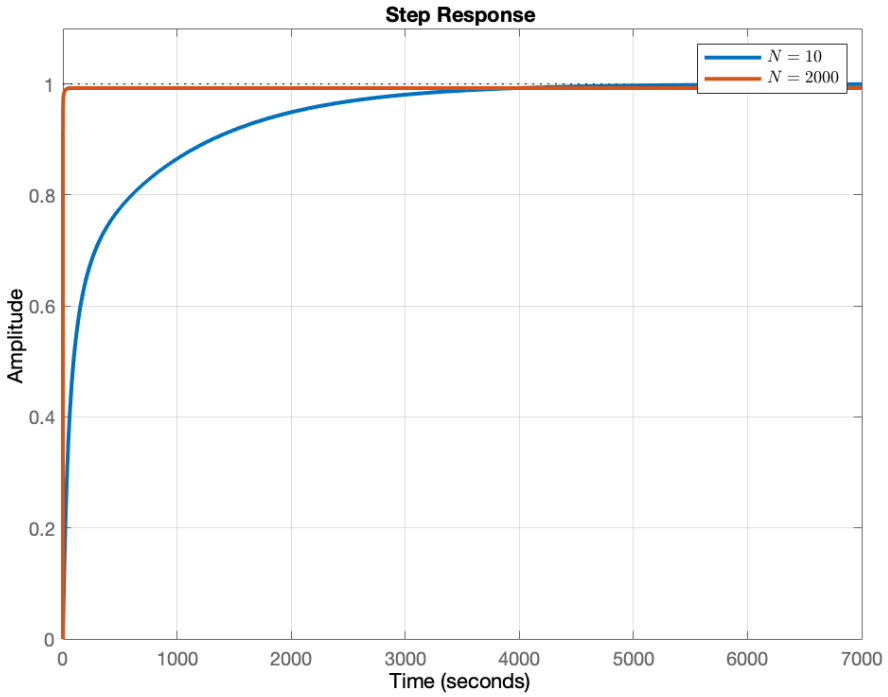


Figure 4.4: A step responses for $N = 10$ and $N = 2000$ at the boundaries.

An examination of the step response can often be helpful to see if the different measurement has asymptotic convergence. Figure 4.4 show a step response for a grid size of $N = 10$ and $N = 2000$, at the boundaries. They are both asymptotically stable however, we can see that the thermal characteristics vary significantly for the same time span. This may lead to an interpretation that a small grid size is asymptotically stable.

We want to ensure a robust method of solving the heat equation, and therefore conclude that this approach had too many uncertainties. In the next chapter, we expand the model to try to account for the solution's stiff part, using a spectral method.

.

# 5 | Spectral method for the 1-D Heat Equation

We want to employ a more stable approach to solve the heat equation. Whereas the finite difference method seeks to approximate the spatial derivatives of its nearest neighbour's, a spectral method will consider the entire global domain. For a small domain, the finite difference method can approximate the solution with relative few grid points. However, it can easily be deduced that expanding the grid size can be computationally expensive for increasing domains and dimensions. In addition, the spectral method converge exponentially [41], thus making it more accurate than the finite difference method. A global method is often preferred for a rapidly varying solution, both in time and space, and can have a high spatial resolution for a long integration time.

The spectral methods require that the solution is sufficiently smooth and piecewise continuous. Therefore, we will recast the general solution into a weak form, and we can expand the solution to a truncated series as a sum of the basis function and an inner product. Witch are orthogonal and forms a complete set.

$$\tau(x,t) = \sum_{j=1}^{\infty} \hat{\tau}_j(t)\phi_j(x) \tag{5.1}$$

## 5.1 Modeling

Let the 1-D heat equation be consider in the region $\mathcal{D} = [0, L]$ where $x \in \mathcal{D}$ $, t \in [0, \infty) \to \mathbb{R}$ be the temperature for a given point $x$ for a time $t$. We can state the heat equation as.

$$\frac{\partial \tau}{\partial t} = \alpha \frac{\partial^2 \tau}{\partial x^2} \tag{5.2}$$

Let the initial condition for the PDE be assumed as a constant temperature distribution for the temperature of the environment.

$$\tau(x,0) = T_{env} \tag{5.3}$$

Heated air/steam and radiative forcing will affect either side of the meat. Therefore, it is assumed that the heat flux at the boundaries satisfies the convective/radiative source at the boundary, which gives the Robin boundary conditions.

$$\begin{aligned} -k\left(\frac{\partial \tau}{\partial x}\right)_0 &= h\left(u-\tau_0\right)+v \\ k\left(\frac{\partial \tau}{\partial x}\right)_L &= h\left(u-\tau_L\right)+v \end{aligned} \tag{5.4}$$

Here, $h$ is the heat transfer coefficient, $u$ is the heated/cooled air temperature that acts on the boundary and $v$ the radiative forcing. The introduction of the Biot number will make the BC dimensionless. The boundary conditions can be recast with the dimensionless Biot number as.

$$\begin{aligned} -L\left(\frac{\partial \tau}{\partial x}\right)_0 &= \mathrm{Bi}\left(u-\tau_0\right)+\frac{L}{k}v \\ L\left(\frac{\partial \tau}{\partial x}\right)_L &= \mathrm{Bi}\left(u-\tau_L\right)+\frac{L}{k}v \end{aligned} \tag{5.5}$$

## 5.2 General solution

We now look for an analytical solution for the homogeneous 1-D heat equation subject to the initial condition and the Robin boundary conditions.

$$\begin{aligned} \frac{\partial \tau}{\partial t}-\alpha\frac{\partial^2 \tau}{\partial x^2} &= 0 \\ -L\left(\frac{\partial \tau}{\partial x}\right)_0+\mathrm{Bi}\tau_0 &= 0 \\ L\left(\frac{\partial \tau}{\partial x}\right)_L+\mathrm{Bi}\tau_L &= 0 \end{aligned} \tag{5.6}$$

The separation of variables principle is used, and we assume that there exists a solution on the form.

$$\tau(t,x)=T(t)X(x) \tag{5.7}$$

The partial derivatives can be written in a more compact notation, where the primes denote a differentiation for a single function.

$$\frac{\partial \tau}{\partial t}=X(x)T'(t) \quad \frac{\partial^2 \tau}{\partial x^2}=X''(x)T(t), \tag{5.8}$$

Inserting this relation into the heat equation, and dividing the equation by $T(t)X(x)$ yields the following factorization.

$$\frac{1}{\alpha}\frac{T'(t)}{T(t)} = \frac{X''(x)}{X(x)} = -\lambda \tag{5.9}$$

The PDE is now separated into two ODE's, with a common factor $\lambda$. The temporal part will only depend on $t$, and the spatial part will only be dependent on $x$. If we have a variation of $t$ and $x$ is fixed, the right-hand side of the equation becomes constant and vice versa. Thus, the common factor $\lambda$ can not be dependent on $x$ or $t$. We can then separate the temporal and spatial equation and rearrange the equation for $T(t)$ and $X(x)$ to solve two different ODE's.

$$T'(t) + \alpha\lambda T(t) = 0 \tag{5.10}$$

$$X''(x) + \lambda X(x) = 0 \tag{5.11}$$

### 5.2.1 Solving for $T(t)$

Solving for $T(t)$ will produce an exponential function of time, dependent on the initial temperature distribution. We only permit stable solutions, which implies that $\lambda > 0$, and the solution is then a decaying exponential function. The choices of the wavenumber $\omega \triangleq \sqrt{\lambda}$ will notationally ensure a stable solution.

$$T(t) = e^{-\omega^2\lambda t}T(0) \tag{5.12}$$

### 5.2.2 Solving for $X(x)$

A general solution for the second-order linear homogeneous ODE can be found in a weak form through the Sturm-Liouville theory. Which requires that the ODE is formulated as the Sturm–Liouville Equations (SLE).

$$\frac{d}{dx}\left[p(x)\frac{dy}{dx}\right] + (q(x) + \lambda w(x))y = 0 \tag{5.13}$$

By recognizing $p(x) = 1$, $q(x) = 0$, $y = X(x)$ and $w(x) = 1$. The spatial equation can be recovered, and classify as an SLE.

However, we will first show that the general analytical solution can be found via inspection and written as a harmonic equation, viz.

$$X(x) = K\cos(\omega x + \psi) \tag{5.14}$$

By consolidating the spatial solution with the Robin boundary condition and dividing by cosine. Yields the following relationship.

$$\begin{aligned} L\omega\tan(\psi) + \mathrm{Bi} &= 0 \\ -L\omega\tan(L\omega+\psi) + \mathrm{Bi} &= 0 \end{aligned} \tag{5.15}$$

The phase can be found by solving

$$\tan(L\omega+\psi) + \tan(\psi) = 0 \Longrightarrow \psi = -\frac{L\omega}{2} \tag{5.16}$$

A relationship for the eigenvalues can be found by inserting the phase back into the boundary conditions. We will show how the eigenvalues may be found in section A.1.

$$L\omega\tan\left(\frac{L\omega}{2}\right) = \mathrm{Bi} \tag{5.17}$$

To attain a weak form of the general solution, we would need the SLE to adhere to the homogeneous Robin boundary condition in the closed interval of $[0, L]$, with $L^2 + \mathrm{Bi}^2 > 0$. The combination of these BC and the SLE is called the Sturm-Liouville problem (SLP).

We can list up three relevant properties to solve this SLP.

- An orthonormal set of the eigenfunctions $\{\varphi_i(x)\}$, can collectively be normalized via the Gram–Schmidt Orthogonalization. Iff. the inner products of the eigenfunctions is orthogonal to each other.

$$\phi_i(x) = \frac{1}{\|\varphi_i\|}\varphi_i(x) \tag{5.18}$$

- An SLP can form a complete set on the interval $x \in [0, L]$ if the eigenfunction is orthogonal to each other.
- There will be a sequence of real and positive eigenvalues, $0 \leq \omega_1 < \omega_2 < \cdots < \omega_i$ that would retain a stable solution to the Sturm-Liouville problem. Which will have an eigenfunctions $\phi_i(x)$ associate with each of the eigenvalues.

$$\langle \phi_i, \phi_j \rangle = \int_0^L \phi_i(x)\phi_j(x)w(x)dx = \delta_{ij} \tag{5.19}$$

The right choice of a Gram–Schmidt Orthogonalization will ensure that a normalised eigenfunction is formed on an orthonormal basis. Let $K$ denote a scaling constant and be chosen such that the integral is unit in the $\mathcal{L}_2([0, L], \mathbb{R})$ norm of the Hilbert space.

$$\sqrt{\int_0^L \cos(\omega x+\psi)^2 dx} = \sqrt{\int_0^L \cos\left(\left(x-\frac{L}{2}\right)\omega\right)^2 dx} = \sqrt{\frac{L\omega+\sin(L\omega)}{2\omega}} \tag{5.20}$$

Denote $K$ as the inverse of the result from the integral.

$$K \triangleq \sqrt{\frac{2\omega}{L\omega + \sin(L\omega)}} \tag{5.21}$$

Verify that the choice of $K$ is normalised.

$$\sqrt{\int_0^L K \cos(\omega x + \psi)^2 dx} = 1 \tag{5.22}$$

Thus, the Gram–Schmidt orthogonalization for an eigenfunction at the $i$'th mode can be written as a cosine centred in the bar, viz.

$$\phi_i(x) = \sqrt{\frac{2\omega_i}{L\omega_i + \sin(L\omega_i)}} \cos\left(\left(x - \frac{L}{2}\right)\omega_i\right) \tag{5.23}$$

### 5.2.3 Orthogonality

We stated that the SLP had to be an orthogonal set of the eigenfunctions, and for the sake of completeness. Let $X_i(x)$ and $X_j(x)$ satisfy the SLP such that.

$$\int_0^L X_i X_j dx = 0 \quad \text{for} \quad i \neq j \tag{5.24}$$

$$X_i''(x) + \lambda_i X_i(x) = 0 \tag{5.25}$$

$$X_j''(x) + \lambda_j X_j(x) = 0 \tag{5.26}$$

With the Robin boundary condition.

$$\begin{aligned} -LX_i'(0) + \mathrm{Bi}\, X_i(0) &= 0 \\ LX_i'(L) + \mathrm{Bi}\, X_i(L) &= 0 \end{aligned} \tag{5.27}$$

$$\begin{aligned} -LX_j'(0) + \mathrm{Bi}\, X_j(0) &= 0 \\ LX_j'(L) + \mathrm{Bi}\, X_j(L) &= 0 \end{aligned} \tag{5.28}$$

Multiplying Equation 5.25 with Equation 5.26 and subtract them from each other, yields.

$$X_j X_i'' - X_i X_j'' + (\lambda_i - \lambda_j) X_i X_j = 0 \tag{5.29}$$

Integrating Equation 5.29 from $[0, L]$ becomes.

$$\int_0^L \left(X_j X_i'' - X_i X_j''\right) dx + (\lambda_i - \lambda_j) \int_0^L X_i X_j dx = 0 \tag{5.30}$$

We will consider the first part of the integral and use integration by parts with the BC. Verify that.

$$\begin{aligned} \int_0^L X_j X_i'' dx &= [X_j X_i']_0^L - \int_0^L X_j' X_i' dx \\ \Rightarrow \int_0^L X_j X_i'' dx &= [X_j(L)X_i(L) - X_j(0)X_i(0)] - \int_0^L X_j' X_i' dx \end{aligned} \tag{5.31}$$

Note how the constant will cancel out. Likewise, for the second part of the integral.

$$\begin{aligned} \int_0^L X_i X_j'' dx &= \left[X_i X_j'\right]_0^L - \int_0^L X_i' X_j' dx \\ \Rightarrow \int_0^L X_i X_j'' dx &= [X_i(L)X_j(L) - X_i(0)X_j(0)] - \int_0^L X_i' X_j' dx \end{aligned} \tag{5.32}$$

Inserting the equations back into Equation 5.30. We can observe how the first integral cancel out viz.

$$(\lambda_i - \lambda_j) \int_0^L X_i X_j dx = 0 \Rightarrow \int_0^L X_i X_j dx = 0 \quad \text{if} \quad n \neq m \tag{5.33}$$

We have numerically determined the eigenvalues for this SLP. In section B.1 one can see the listing for the code with a numerical calculation that verifies that this problem is orthogonal.

### 5.2.4 Full solution

Since the eigenfunctions are orthogonal, and the SLP can form a complete set over the interval $[0, L]$, i.e. they can approximate the function over the global domain. They can be used in much the same way as Fourier series for sin and cos. Let the expansion coefficients of $\tau$ be defined by.

$$\tau_j = \int_0^L \phi_j \tau dx \tag{5.34}$$

A linear PDE can be superimposed with an arbitrary accuracy with a truncated sum.

$$\tau = \sum_{i=1}^{n} \phi_i \tau_i = \sum_{i=1}^{n} \phi_i(x) e^{-\alpha \omega_i^2 t} \tag{5.35}$$

Thus, the general solution for the homogeneous PDE can be written as.

$$\tau(x,t) = \sum_{i=1}^{\infty} \int_0^L \phi_i(x)\phi_j\left(x'\right) e^{-\alpha\omega_i^2 t} \tau\left(x',0\right) dx' \tag{5.36}$$

## 5.3 Weak formulation

The SLP will be formulated from a strong form to a generalized solution (a weak form). The strong form is governed by the PDE, and the associated BC. Recall from the derivation of the heat equation. We asserted that Newton's law of cooling described a relationship between the heat flux at the boundary and the object's interior, which requires the function to be smooth. This property may cause some issue: If the function at the boundary is not sufficient smooth enough over the boundary, e.g. from a high/low-temperature spike. The PDE can become too strict, and a physical solution can not be obtained. Consequently, the spatial derivative may not be evaluated numerically at the boundary.

By formulating the PDE to a weak form, we can mitigate the aforementioned problem. A weak formulation will essentially recast the PDE to an integral form and the second derivative to a less strict form. Which will make the PDE more subjective to extensive changes on the boundary. Hence, we are ensured that a numerical solution can be found at the boundary with a high/low-temperature spike.

Let the weak form of the heat equation be integrated over the region $x \in [0, L] \to \mathbb{R}$. With a test function be denoted by the eigenfunction $\phi_i$ subject to the same region. Then, we can integrate the product of $\phi_i \cdot \tau$ over the global domain. If $\tau$ is a solution, each mode to the eigenfunctions will fix the solution to zero; then it must hold that.

$$0 = \int_0^L \phi_i \left( \frac{\partial \tau}{\partial t} - \alpha \frac{\partial^2 \tau}{\partial x^2} \right) dx \tag{5.37}$$

By using the product rule, the spatial derivation may be recast as follows.

$$\phi_i \frac{\partial^2 \tau}{\partial x^2} = \frac{\partial}{\partial x}\left( \phi_i \frac{\partial \tau}{\partial x} \right) - \frac{\partial \tau}{\partial x}\frac{\partial \phi_i}{\partial x} = \frac{\partial}{\partial x}\left( \phi_i \frac{\partial \tau}{\partial x} - \tau \frac{\partial \phi_i}{\partial x} \right) + \tau \frac{\partial^2 \phi_i}{\partial x^2} \tag{5.38}$$

Integration by parts will produce an alternative form of the weak equation.

$$\int_0^L \phi_i \frac{\partial \tau}{\partial t} - \alpha \frac{\partial^2 \phi_i}{\partial x^2} \tau dx = \alpha \left[ \phi_i \frac{\partial \tau}{\partial x} - \tau \frac{\partial \phi_i}{\partial x} \right]_0^L dt \tag{5.39}$$

It can be noted how the weak form will naturally produce the Robin boundary condition. The weak formulation can be simplified by using the properties of

the eigenfunction[1], Verify that Right-hand side of the integral becomes.

$$\int_0^L \phi_i \frac{\partial \tau}{\partial t} - \alpha \frac{\partial^2 \phi_i}{\partial x^2} \tau dx = \int_0^L \phi_i \left( \frac{\partial \tau}{\partial t} + \alpha \omega_i^2 \tau \right) dx \tag{5.40}$$

The weak formulation will ensure that the eigenfunctions will satisfy the temperature distribution at the boundary as well as homogeneous ones; thus, we can deduced that.

$$\begin{aligned}
\left[ \phi_i \frac{\partial \tau}{\partial x} - \tau \frac{\partial \phi_i}{\partial x} \right]_0^L &= \left( (\phi_i)_L \left( \frac{\partial \tau}{\partial x} \right)_L - \tau_L \left( \frac{\partial \phi_i}{\partial x} \right)_L \right) - \left( (\phi_i)_0 \left( \frac{\partial \tau}{\partial x} \right)_0 - \tau_0 \left( \frac{\partial \phi_i}{\partial x} \right)_0 \right) \\
&= (\phi_i)_L \frac{1}{L} \left( L \left( \frac{\partial \tau}{\partial x} \right)_L + \mathrm{Bi} \tau_L \right) - (\phi_i)_0 \frac{1}{L} \left( L \left( \frac{\partial \tau}{\partial x} \right)_0 - \mathrm{Bi} \tau_0 \right) \\
&= (\phi_i)_L \frac{1}{L} \left( \mathrm{Bi} u + \frac{L}{k} v \right) + (\phi_i)_0 \frac{1}{L} \left( \mathrm{Bi} u + \frac{L}{k} v \right) \\
&= \frac{(\phi_i)_L + (\phi_i)_0}{L} \left( \mathrm{Bi} u + \frac{L}{k} v \right)
\end{aligned} \tag{5.41}$$

The weak formulation for the homogeneous SLP will reduce to.

$$\int_0^L \phi_i \left( \frac{\partial \tau}{\partial t} + \alpha \omega^2 \tau \right) dx = \left( (\phi_i)_L + (\phi_i)_0 \right) \frac{\alpha}{L} \left( \mathrm{Bi} u + \frac{L}{k} v \right) \tag{5.42}$$

We will denote $b_i$ as the i'th mode of the eigenfunction for later use.

$$b_i \triangleq (\phi_i)_L + (\phi_i)_0 = 2 \cos\left( L \omega_i / 2 \right) \sqrt{\frac{2 \omega_i}{L \omega_i + \sin\left( L \omega_i \right)}} \tag{5.43}$$

## 5.4 Discretization

We want to discretize the weak formulation of the Sturm-Liouville problem in order to simulate the solution. Let the model expansion of $\tau$ be inserted back into the weak formulation. Recognizing that the eigenfunctions are orthonormal. A decoupled system of ODE's can be written as.

$$\frac{\partial \tau_j}{\partial t} + \alpha \omega_j^2 \tau_j = \frac{b_i}{L} \left( \mathrm{Bi} u(t) + \frac{L}{k} v \right) \tag{5.44}$$

Denoting the state vector as.

[1] $\frac{d}{dx} f(x) = \lambda f(x)$, if the eigenfunctions are differentiated twice, it can be the product of the eigenvalues squared multiplied by the eigenfunctions

$$\boldsymbol{\tau} \triangleq \begin{bmatrix} \tau_1 \\ \tau_2 \\ \vdots \\ \tau_i \end{bmatrix} \tag{5.45}$$

Let $\boldsymbol{\Lambda}$ be diagonal matrix containing $\Lambda_{ii} = -\alpha\omega_i^2$ on each of the diagonal position. In addition, let $\boldsymbol{b}$ denote a vector that contains the controller input $b_i$. Then a state-space formulation can be represented by the linear model.

$$\dot{\boldsymbol{\tau}}(t) = \boldsymbol{\Lambda}\boldsymbol{\tau}(t) + \boldsymbol{b}\alpha\left(\frac{\mathrm{Bi}}{L}u(t) + \frac{1}{k}v(t)\right) \tag{5.46}$$

The outputs for the model can be found by utilizing the eigenfunctions, and measurement at $x = x_m$ is found by.

$$y(t) = \sum_{i=1}^{n} \phi_i\left(x_m\right)\tau_i(t) = \boldsymbol{c}\boldsymbol{\tau}(t), \quad c_i = \phi_i(x) \tag{5.47}$$

## 5.5 Preliminary simulation validation for an edge case

The preliminary result for the spectral method is simulated in MATLAB and can be seen Figure 5.1. The simulation parameters can be found in Table 5.1.

| Symbol | Variable | Value | Unit |
|---|---|---|---|
| L | Length | 5 | $[cm]$ |
| $\alpha$ | Thermal diffusivity | $1.3e-7$ | $[m^2/s]$ |
| Bi | Biot number | 140 | $[-]$ |
| $\tau(x,0)$ | Initial/-Room Temperature | 20 | $[^\circ C]$ |
| $\tau_{cutoff}$ | Internal core temperature | 65 | $[^\circ C]$ |

Table 5.1: Parameter values for the preliminary simulation of the spectral method of the the 1-D heat equation.

The step function for the simulated heat source is given below.

$$u(t) = \begin{cases} 200 & \text{if } \tau(L/2,t) \leq \tau_{cutoff} \\ 20 & \text{if } \tau(L/2,t) > \tau_{cutoff} \end{cases} \tag{5.48}$$

The spectral method model is tested against the same conditions as the Finite-difference model from section 4.4 and showcase much of the same characteristics as the first model. Which can be seen in Figure 5.1b. The input source heats up the object's boundaries, and the temperature starts to propagate

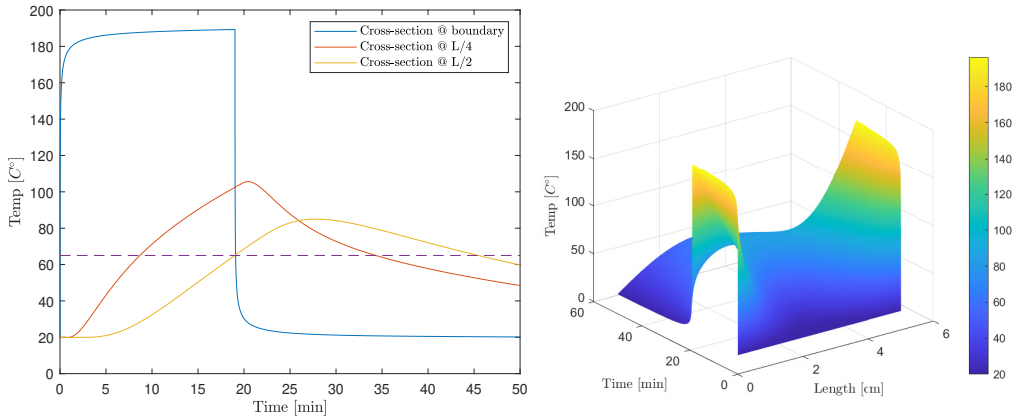


(a) A 2-d plot of three cross-sections. (b) A 3-d Plot of the simulation.

Figure 5.1: Preliminary simulation validation for an edge case for the spectral method.

throughout the simulated meat. The interior of the simulated meat has a slower convergence rate compared to the sides, and at $t \approx 20[min]$ the core of the meat reaches $\tau_{cutoff}$ as seen in Figure 5.1a. Since Bi $\gg 1$ The Robin boundary condition reduces almost to Dirichlet boundary condition, and the conductive heat source is the dominating factor. It can be observed that the curvature of the boundary is not as steep as the Finite-difference model, most likely since we have a small effect from the Neumann condition.

Examining Figure 5.2a we can observe how the solution is approximately the same with relative few modes. For $N < 20$ the dynamics is slightly off, however when $t \approx 20[min]$ (same as $\tau_{cutoff}$). Will the spectral method seek a global solution, and the system converges together. We can further observe from Figure 5.2b that we would need a large number of modes ($N \geq 500$) to achieve an acceptable approximation tolerance at the boundaries. One key difference with this model is that the model's dynamic is not affected by low numbers of modes, only the amplitude. This was an issue with the Finite-difference model; it would have different dynamics for different magnitudes of the stencils.

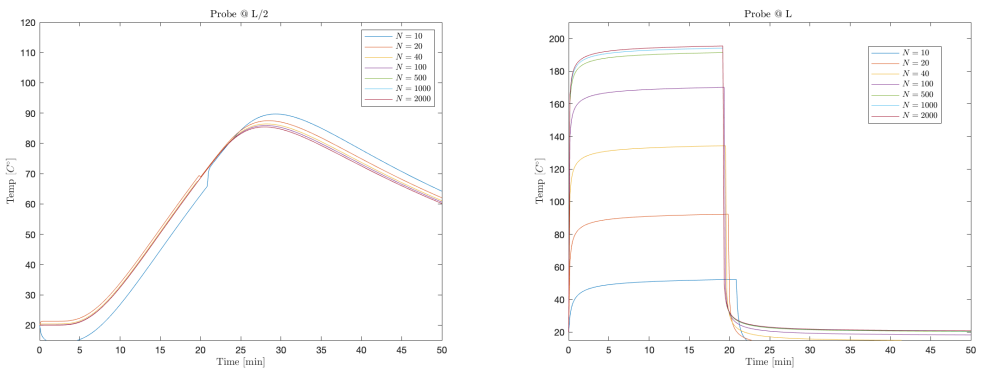


(a) A cross-section at the center. (b) A cross-section at the boundary.

Figure 5.2: Two plots that showcase different resolution with different modes.

When solving for $\tau(x,t)$, we end up with an analytical solution containing a cosines function and an exponential function in time. The spectral method works in much the same way as a Fourier series, where we use a series of cosine function to estimate the heat equation. When we use this global method to approximate the heat equation, we know that any error in the model has to be a function of the non included modes (same as a Fourier series). Suppose we choose the modes to be 10. We would know the residual error is a linear combination of the non-included modes $11, 12, 13, \ldots N$. Increasing the set of modes will improve the resolution because we account for a tighter set of amplitudes and frequencies changes [2]. The choice of modes can then be determined by inspecting the step response of the PDE. Knowing that if the amplitude converges asymptotically to 1 for each mode, the number of modes is well chosen. Figure 5.3 shows that the characteristic is identical at the boundaries. Only the amplitude differs for a low and high number of modes.

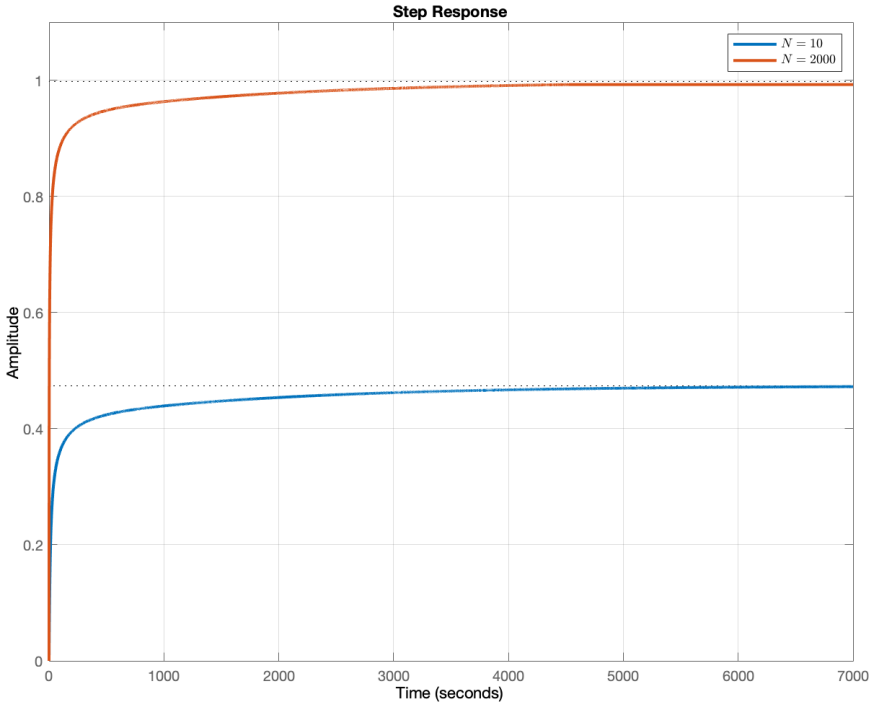


Figure 5.3: Step responses to show that the amplitudes changes for $N = 10$ and $N = 2000$, for high a Bi value.

Figure 5.4 shows the heat equation subject to different values of the dimensionless Biot coefficient. This is done to verify that the Robin boundary condition works properly. It can be observed that a low value, $\text{Bi} = 0.1$. The system can be seen as insulated, and the Robin boundary condition reduces to the Neumann condition. Which slows temperature propagation from the heat source

[2] In the spatial axis, a sinusoidal curve was the solution to the heat equation. Which propagates amplitudes in the temporal direction.

at the boundaries. When Bi becomes higher, Bi = 4 and Bi = 40, the Robin boundary condition is a mixed case. The system can be seen as less insulated from the contribution of the Neumann condition. It makes sense that heat would propagate at a slower rate at the boundary for a low value of Bi. As we increase the value of Bi = 140, the system's boundary is more receptive to heat flux. This entails that the Dirichlet condition becomes dominating.

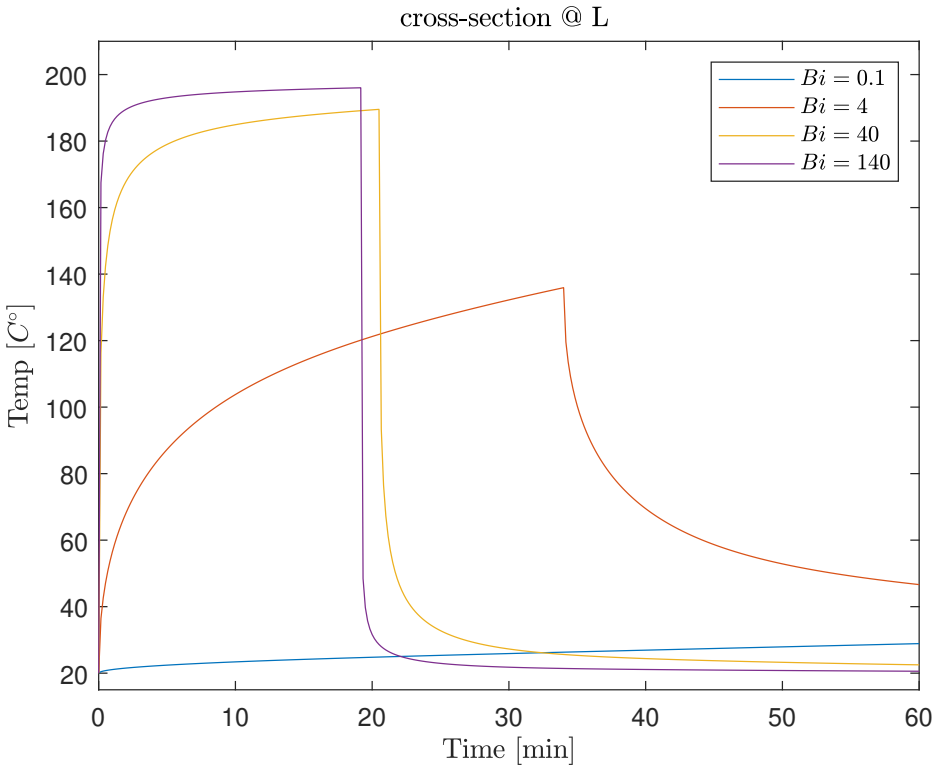


Figure 5.4: A 2-d plot of four cross-sections. Showcasing different Biot values.

We will conclude that the spectral model is more robust compared to the finite differences model—expensive inverse operation from the system matrix, **A** are not needed. A global solution will ensure exponential convergence and high spatial resolution for a long integration time. Residual error in the modes can be found by examining the step response.

We have only operated in one dimension to this point, which will not be a practical approximation to a physical heat distribution problem. We will expand the spectral method into cylindrical coordinates, examine a uniform disk, and conceptualize the one-dimensional cases as proof of concept. In addition, we have not included a controller for the problem to reach an idealized temperature profile for the meat. The next chapter will introduce the method to predict the controller input via a model predictive control.

# 6 | Model Predictive Control

We want to establish a method to control a convective/radiative heat source. Such that the temperature distribution in the meat does not exceed the idealized temperature profile. This thesis proposes that a Model Predictive Control (MPC) may find an optimal control sequence. Contrary to stander cooking techniques of measuring the temperature at the centre of a roast. Will this thesis assume a measurement is at the centre of a roast and let the spectral model facilitate a set of output measurements. Which are then constrain to idealized doneness. This may ensure that an idealized temperature profile throughout the roast can be achieved.

## 6.1 MPC with Reference Tracking

The MPC feedback controller utilizes the dynamics from the model to forecast the dynamical behaviour of the model. It solves an optimized sequence of control action, based on the recent and predictive action of the model [42, 43, 44]. This makes the MPC dependent on an accurate model. However, it can allow small degree of model plant mismatch [45]. The predictive action is dependent on the inputs from the model and the measured outputs over a discrete-time span $t \in [0 \dots p]$. Here $p$ is commonly referred to as the prediction horizon. To obtain the control sequence, we minimizing a cost function subject to a set of constraints inside a feasible set. The MPC algorithm will calculate the control sequence over a prediction horizon, using the first move as the next input, and rejects the remaining control sequence. The re-optimization is done repeatedly for $0 \leq \Delta t \leq t_{end}$. Shifting the prediction horizon for each time-step $\Delta t$ and reinitialize the optimization scheme.

The MPC optimizing strategy has some beneficial properties that may produce an idealized temperature profile for a slab of meat.

- MPC may interact with a multi-input multi-output (MIMO) system. Since we are considering a convective/radiative heat source, we only have one input variable, making the plant a single-input multiple-output (SIMO) system.
- The possibility of implementing constraints on the Manipulated Variable (MV) and the Output Variables(OV).
- Minimizing the error reference tracking for a feasible set of measured outputs in the meat.

### 6.1.1 Cost Function

This thesis uses Matlab to simulate the optimal controller sequence of the proposed spectral model. The MPC will be designed with the "Model predictive control toolbox™" from Matlab [46]. The MPC toolbox needs an LTI plant in the form of a state-space representation. Given the plant model, a linear discrete state-space formulation can be on the form.

$$\begin{aligned} \boldsymbol{x_{k+1}} &= \boldsymbol{A}\boldsymbol{x_k} + \boldsymbol{B}\boldsymbol{u_k} \\ \boldsymbol{y_k} &= \boldsymbol{C}\boldsymbol{x_k} + \boldsymbol{D}\boldsymbol{u_k} \end{aligned} \tag{6.1}$$

Here, $\boldsymbol{x_k} \in \mathbb{R}^n$, $\boldsymbol{y_k} \in \mathbb{R}^q$ and $\boldsymbol{u_k} \in \mathbb{R}^m$ is respectively the state vector, output vector and the control input for a current control interval $k$. The state matrix $\boldsymbol{A} \in \mathbb{R}^{n\times n}$ and the input matrix $\boldsymbol{B} \in \mathbb{R}^{n\times m}$, are assumed to be constant, and the output vector is a linear combination of the state vectors and the controller inputs, $\boldsymbol{C} \in \mathbb{R}^{q\times n}$. We will assume that there is no direct feedthrough, i.e. $\boldsymbol{D} = 0$.Thus, we can write the regulation error for the plant as a linear combination of a reference tracking vector, the output variable and manipulated variable.

$$\begin{aligned} \boldsymbol{e}_y(i+k) &= [\boldsymbol{r}(k+i+1 \mid k) - \boldsymbol{y}(k+i+1 \mid k)] \\ \Delta u(k+i) &= [u(k+i \mid k) - u(k+i-1 \mid k)] \end{aligned} \tag{6.2}$$

Let, $p$ be defined as the prediction horizon, for $i = [0, \ldots, p-1]$. With, $\boldsymbol{r}$ as the outputted reference values for the i'th prediction horizon at an input instance $k$. Then, for a finite prediction horizon, we need the cost function to minimize the regulation error. Let the cost function be defined as.

$$\begin{aligned} J\left(\boldsymbol{z_k}\right) = \sum_{i=0}^{p-1} \left[\boldsymbol{e}_y^T(k+i)\mathcal{Q}\boldsymbol{e}_y(k+i)\right] + \left[\Delta u^T(k+i)\mathcal{R}_{\Delta u}\Delta u(k+i)\right] + \mathcal{S}\epsilon^2 \\ \text{Where} \\ \boldsymbol{z_k}^T = \left[u(k \mid k)^T u(k+1 \mid k)^T \cdots u(k+p-1 \mid k)^T \;\; \epsilon_k\right] \end{aligned} \tag{6.3}$$

$\mathcal{Q} \in \mathbb{R}^{q\times q}$ and $\mathcal{R}_{\Delta u} \in \mathbb{R}^{m\times m}$ are diagonal penalty weights matrices. That will acts as the cost parameters for the states and the controller input respectively. The weight matrices are chosen such that they are positive-definite, $\mathcal{Q} \succeq 0,\ \mathcal{R}_{\Delta u} \succeq 0$. In addition, we soften the objective function by introducing a slack variable $\epsilon$ with a diagonal constraint violation penalty weight matrices, which are positive-definite $\mathcal{S} \succeq 0$.

### 6.1.2 Constraints

The constraints will ensure that we do not violate any infeasible actions and produce an idealized temperature profile for a slab of meat. Realizing this

problem will require to imposes some constriction on the system. These are as follows.

- A state-space reparation of the temperature dynamics.
- The initial temperature profile of the states and the last move from the convective/radiative source.
- The maximum and minimum allowed output measurement for the temperature at the i'th mode.
- The maximum and minimum temperature a convective/radiative source can emit.
- The temperature rate of change from the convective/radiative source.
- A slack variable that ensures the hard constraints can sometimes be violated and a solution is feasible.
- A vector of reference tracking to reach an idealized temperature profile.

Which can be described by the following equations.

$$\begin{aligned} \boldsymbol{x_{k+1}} &= \boldsymbol{A x_k} + \boldsymbol{B u_k} \\ \boldsymbol{x_0},\ u_{k-1} &= \text{ given} \\ \boldsymbol{y}_k^{\text{low}} - \epsilon &\leq \boldsymbol{y}_k \leq \boldsymbol{y}_k^{\text{high}} + \epsilon \\ u_k^{\text{low}} - \epsilon &\leq u_k \leq u_k^{\text{high}} + \epsilon \\ -\Delta u_k^{\text{low}} - \epsilon &\leq \Delta u_k \leq \Delta u_k^{\text{high}} + \epsilon \end{aligned} \tag{6.4}$$

It can be noted that the heat equation is governed by the maximum principle, which assures temperature is inside the region of interest and will propagate to the maximum/minimum temperature outside, when $t \to \infty$. Thus, the feasible solution must be found in the domain of the active set of the MV.

## 6.2 Case Study of the 1-D Heat Equation with an MPC Strategy

The case study uses the MPC optimization strategy to control the 1-D heat equation with the spectral method to constrain the temperature distribution at four different measurements. The aim is to try out two different Biot numbers and inspect the optimized controller sequence. The controller sequence will be initiated at room temperature to observe how the sequence would evolve in time and temperature. From this, we can deduce which temperature a convective/radiative heat source may be set to.

For this case study, we will assume the following in Table 6.1. Note that the assumption of the manipulated variables, constraints the inequality inside the outputted variables domain, i.e. $\arg\min\{u_k\} \leq \arg\min\max\{y_k\} \leq \arg\max\{u_k\}$.

In addition, we assume that there is integrated white noise in the output variables and no blockage moves from $u$. The input rates were chosen to generate heat faster and dissipate at a slower rate, which can be seen as a likely scenario for a oven.

| **Symbol** | **Variable** | **Value** | **Unit** |
|---|---|---|---|
| L | Length | 5 | $[cm]$ |
| $\alpha$ | Thermal diffusivity | $1.3e-7$ | $[m^2/s]$ |
| $\tau_{med}$ | Medium doneness | 55 | $[°C]$ |
| $\tau_{max}$ | Max allowed temperature | 75 | $[°C]$ |
| $p$ | Prediction horizon | 200 | $[-]$ |
| $x_0$ | Initial temp. distribution | 20 | $[°C]$ |
| $u_{k-1}$ | Last move of the input | 20 | $[°C]$ |
| $y_k^{\text{low}}, y_k^{\text{high}}$ | Min & max temp. to OV | $[20, 75]$ | $[°C]$ |
| $u_k^{\text{low}}, u_k^{\text{high}}$ | Min & max temp. to MV | $[20, 250]$ | $[°C]$ |
| $\Delta u_k^{\text{low}}, \Delta u_k^{\text{high}}$ | Min & max temp. rate to MV | $[-0.25, 0.5]$ | $\left[\frac{°C}{s}\right]$ |

Table 6.1: Parameter values for the case study the one-dimensional heat equation with an MPC strategy.

The heat equation's physic dictates how heat enters the boundary and goes towards equilibrium for $t \to \infty$. Since heat enters at the boundary we allow for higher reference error closer to the edges and accept tenderness decrease for $x_k < L_{0.15}$ and $x_k > L_{0.85}$, i.e. 15% and 85% of the length. Subsequently, the reference vector $\boldsymbol{r}_k$ can be model with the function below.

$$\boldsymbol{r}_k = \begin{cases} \tau_{med} & \text{if} \quad L_{0.15} \leq x_k \leq L_{0.85} \\ \tau_{max} - a \cdot \tau_{med} & \text{if} \quad x_k < L_{0.15} \\ \tau_{med} + b \cdot \tau_{max} & \text{if} \quad x_k > L_{0.85} \end{cases} \tag{6.5}$$

Where $a$ and $b$ are scaling coefficients for $t \in [0, i/3]$. The function for $\boldsymbol{r}_k$ can be seen in Figure 6.1.

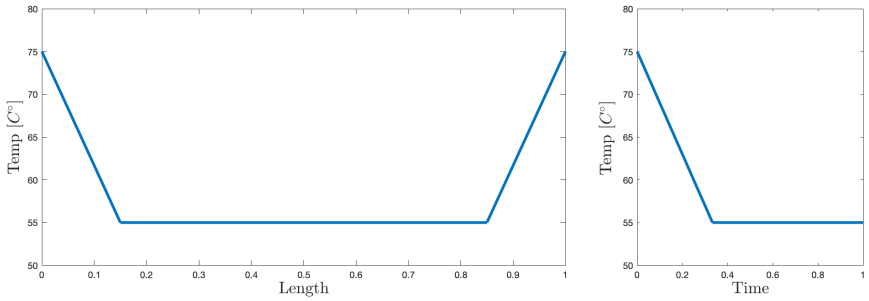


Figure 6.1: The 3-D reference variable $\boldsymbol{r}_k$ visualised, with two 2-D plots.

### 6.2.1 Simulation

Three validation test was performed numerically in Matlab. First, the penalty weights were tested if they are a positive-definite Hessian. Which will ensure a unique solution is feasible. Both plants had positive-definite Hessian for the OV's and MV's. Secondly, the systems were tested for closed-loop internal stability. The eigenvalues for both plants was found tightly spaced and less than zero. Making the plants internally stable for each of the controller modes and can be seen as pure integrators. Thirdly, hard & soft constraints are visually inspected and found in the MV's active set. In real-time usage, the heat source may be perturbed or start to fluctuate. To compensate for this behaviour, an added slack are imposed on the MV's and OV's. This will ensure that the problem does not become infeasible.

The following values was used for the penalty matrices $\mathcal{Q} = diag([2\ \ 2\ \ 1\ \ 1])\beta$ and $\mathcal{R}_{\Delta u} = 0.1/\beta$. For the measured output vector $\boldsymbol{y_k} = [0, 0.75, 1.25, 2.5]^T$. Where, $\beta$ is an overall adjustment factor applied to the weights. The first simulation was done with a Biot value of Bi = 1.

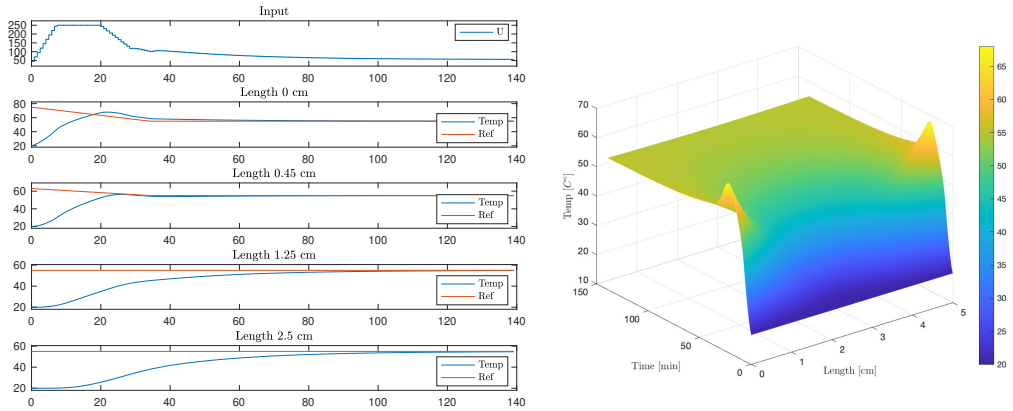


(a) A 2-d plot of four cross-sections with the constraints for the MPC and the corresponding input sequence.

(b) A 3-d plot of the simulated run. For a rod with length $0 \leq x \leq 5$

Figure 6.2: The MPC strategy with the 1-d heat equation with a Bi = 1.

Figure 6.2 shows that the MPC strategy seeks to find the optimum. It pushes the system to build up the maximum allowed temperature at the fastest permitted rate. Such that maximum thermal energy can diffuse into the system at the start of the simulation. The MPC holds the maximum allowed temperature for 15 minutes before letting the heat dissipate. First fast, then slowly to a steady-state temperature of $\tau_{med}$ at $t \approx 110\ [min]$.

We can observe that the boundaries have a slight overshoot at $L = 0$ with a peak of $67°C$. Due to how we choose the reference vector, $\boldsymbol{r_k}$, we did not exceed $\tau_{max}$ and we did not need to penalize the system at $L = 0$ too high. Potential making the plant give a more sluggish controller response. However the rest of the measurement, $L = 0.45$, $L = 1.25$ and $L = 2.5$ tract the reference vector consistently. Which gives medium doneness for at least 70% of the meat.

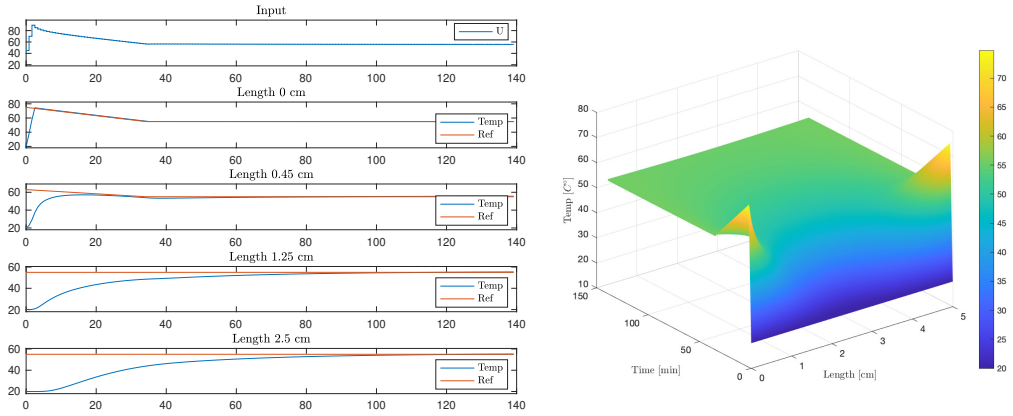


(a) A 2-d plot of four cross-sections with the constraints for the MPC and the corresponding input sequence.

(b) A 3-d plot of the simulated run. For a rod with length $0 \leq x \leq 5$

Figure 6.3: The MPC strategy with the 1-d heat equation with a Bi = 40.

For the second simulation, Bi $= 40$. The weight matrix was changed to $\mathcal{Q} = diag([80 \quad 40 \quad 1 \quad 1])\beta$. We can observe that we had to substantially increase the penalty to track the reference at $L = 0$ and $L = 0.45$. As seen in Figure 6.3. The increased penalty comes from the internal conductive resistances in the object is relatively high. It will be more susceptible to thermal energy, and heat will flow in large quantity at the boundaries. Which makes the temperature spike up to $\tau_{max}$ at $t \approx 3$ $[min]$. However, the system tracks all the measurement consistently at a potential cost of giving a sluggish controller response and $\tau_{med}$ is reach for 70% of the length.

Furthermore, we can observe that the optimized input give a peak temperature of $90°C$, which is less than the previous simulation. The input sequence gives the same thermal characteristic as a low Biot number, and a steady-state temperature is achieved after $t \approx 90[min]$.

We optimize for temporal properties and not the transit behaviour and this case study will conclude that: Starting at the maximum allowed temperature is a sound strategy for a low Biot number. This will reduce the time it takes to reach the idealized temperature profile. For higher Biot numbers, it would be prudent to start at a lower temperature setting for a convective/radiative heat source.

# 7 The Spectral Method for the 2-D Heat Equation

The one-dimensional heat equation was a valuable way of showing how the physic works and validate the different approaches. By extending into a two-dimensional system, we may get a more realistic system contrary to the one-dimensional case. We will use the same approach from chapter 5 to seek a solution for a symmetric disk. Assuming the convective/radiative heat source is more prominent over the radial surface to the vertical surface. Figure 7.1 depicts a geometrical differential control volume we want to model. The control volume is characterized by the dimensions $dz$ in the vertical direction, $dr$ in the radial direction and $rd\varphi$ in the angular direction.

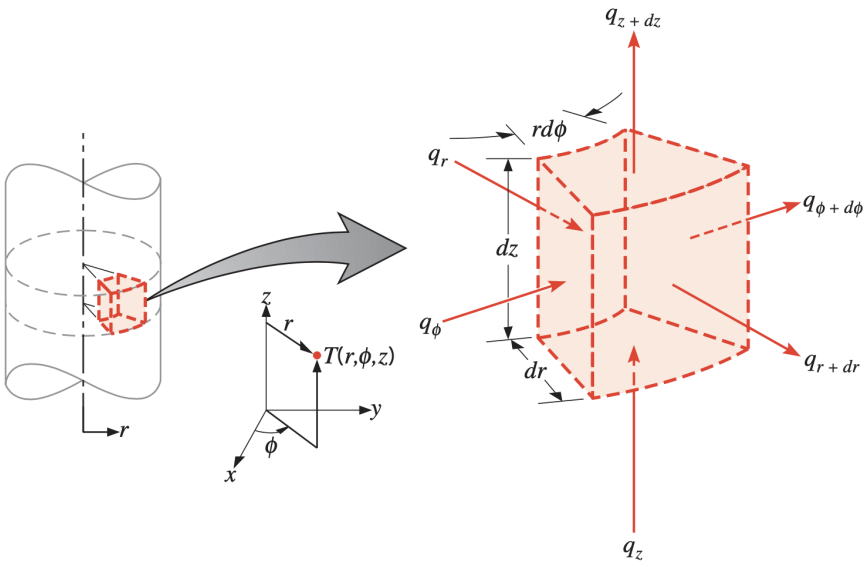


Figure 7.1: Differential control volume from the book *Fundamentals of heat and mass transfer* [47].

## 7.1 Modeling

The one-dimensional heat equation will be extended into cylindrical coordinates such that a disk with angular symmetry can be considered. Let the domain for the radius be denoted as $0 \leq r \leq a$. For a given temperature profile, let $\tau : [0, a] \times [0, \infty) \mapsto \mathbb{R}^2$ at location $r$ and time $t$.

The heat equation for a cylindrical system may be derived by studying the energy balance around a differential element, with the assumption of no internal heat generation.

$$\dot{E}_{\text{stored}} = \dot{E}_{\text{in}} - \dot{E}_{\text{out}} \tag{7.1}$$

The stored energy is proportional to the mass, the heat capacity $c_p$ and the temperature rate, where we can relate the mass with the density $\rho$ times the volume.

$$\dot{E}_{stored} = \rho c_p \frac{\partial \tau}{\partial t} \cdot drdzrd\varphi \tag{7.2}$$

The energy that enters and leaves the differential element can be related by.

$$\dot{E}_{\text{in}} - \dot{E}_{\text{out}} = (q_r + q_\varphi + q_z) - (q_{r+dr} + q_{\varphi+d\varphi} + q_{z+dz}) \tag{7.3}$$

By using the Taylor expansion, we can recast the energy leaving the control volume.

$$\begin{aligned} \text{Radial: } q_{r+dr} &= q_r + \frac{\partial q_r}{\partial r} dr \\ \text{Angular: } q_{\varphi+d\varphi} &= q_\varphi + \frac{\partial q_\varphi}{\partial \varphi} d\varphi \\ \text{Axial: } q_{z+dz} &= q_z + \frac{\partial q_z}{\partial r} dz \end{aligned} \tag{7.4}$$

By combining Equation 7.2 and the recast form of Equation 7.3 we can assert the following relationship. Where, the left side is the energy storage term, and the right side represents the net rate at which energy enters the control volume.

$$\rho c \frac{\partial \tau}{\partial t} drdzrd\varphi = -\frac{\partial qr}{\partial r} dr - \frac{\partial q\varphi}{\partial \varphi} d\varphi - \frac{\partial qz}{\partial z} dz \tag{7.5}$$

The flow of energy through the control volume can be related to Fourier's law. Such that heat flux acting on an element is proportional to temperature gradient times the cross-sectional area.

$$\begin{aligned} \text{Radial: } q_r &= -k \frac{\partial \tau}{\partial r} rd\varphi dz \\ \text{Angular: } q_\varphi &= -k \frac{\partial \tau}{r \partial \varphi} drdz \\ \text{Axial: } q_z &= -k \frac{\partial \tau}{\partial z} rd\varphi dr \end{aligned} \tag{7.6}$$

Combining the preceding equation yields the complete heat equation in cylindrical coordinates.

$$\rho c_p \frac{\partial \tau}{\partial t} = \frac{1}{r}\frac{\partial}{\partial r}\left(kr\frac{\partial \tau}{\partial r}\right) + \frac{1}{r^2}\frac{\partial}{\partial \varphi}\left(k\frac{\partial \tau}{\partial \varphi}\right) + \frac{\partial}{\partial z}\left(k\frac{\partial \tau}{\partial z}\right) \tag{7.7}$$

By imposing angular symmetry and inspecting a cross-section with width $dz$. We can simplify the heat equation.

$$\frac{\partial \tau}{\partial t} = \alpha \frac{1}{r}\frac{\partial}{\partial r}\left(r\frac{\partial \tau}{\partial r}\right), \quad \alpha \triangleq \frac{k}{\rho c_p} \tag{7.8}$$

The exterior of the cylinder will be exposed to a convective heat source or radiative forcing. By utilizing the second law of thermodynamics, we can assume that the flux on the boundary is proportional to the difference between the environment and the object, viz.

$$q_a = hA\left(u - \tau_a\right) + v \tag{7.9}$$

Where $u$ denotes the air temperature, $A$ cross-sectional area, $v$ the radiative forcing and $h$ the heat transfer coefficient. The boundary conditions can be related to the radial heat flux from Equation 7.6 and the interface from Equation 7.9 yielding a Robin condition for the problem [1].

$$-k\left(\frac{\partial \tau}{\partial r}\right)_a = h\left(u - \tau_a\right) + v \tag{7.10}$$

By combining Equation 7.10 with the dimensionless Biot number, we get the following relationships for the boundary condition.

$$L_c\left(\frac{\partial \tau}{\partial x}\right)_a = \mathrm{Bi}\left(u - \tau_a\right) + \frac{L}{k}v \tag{7.11}$$

# 7.2 General Solution

We recover the heat equation and recasting it to an easier form to work with.

$$\begin{aligned} &\frac{\partial \tau}{\partial t} = \alpha \frac{1}{r}\frac{\partial}{\partial r}\left(r\frac{\partial \tau}{\partial r}\right) \\ \Leftrightarrow\ &\frac{\partial \tau}{\partial t} - \alpha\left(\frac{\partial^2 \tau}{\partial r^2} + \frac{1}{r}\frac{\partial \tau}{\partial r}\right) = 0 \end{aligned} \tag{7.12}$$

Subjected to the homogeneous, linear Robin boundary conditions.

[1] Note: The cross-sectional area A gets cancelled out.

$$L_c \left( \frac{\partial \tau}{\partial r} \right)_a + \mathrm{Bi}\, \tau_a = 0 \tag{7.13}$$

In order to solve the PDE into a set of ODE's, separation of variables is used. We assume the solution is on the form.

$$\tau(t, r) = T(t)R(r) \tag{7.14}$$

Inserting the factorization into the heat equation and dividing with $T(t)R(r)$ on both sides of the equation, the separated equation becomes.

$$\begin{aligned} \frac{1}{\alpha}\frac{\partial T}{\partial t}R &= T\frac{\partial^2 R}{\partial r^2} + T\frac{1}{r}\frac{\partial R}{\partial r} \\ \Leftrightarrow \frac{1}{\alpha}\frac{1}{T}\frac{\partial T}{\partial t} &= \frac{1}{R}\left( \frac{\partial^2 R}{\partial r^2} + \frac{1}{r}\frac{\partial R}{\partial r} \right) \end{aligned} \tag{7.15}$$

A separation constant can be found, which are not dependent on $r$ and $t$ such that both sides will be equal. Let it be defined as $-\lambda^2$. This yields a temporal ODE on the form.

$$\frac{\partial T}{\partial t} + \alpha\lambda^2 T = 0 \tag{7.16}$$

The temporal part has an well-know analytical solution, viz.

$$T(t) = e^{-\alpha\lambda^2 t}T(0) \tag{7.17}$$

### 7.2.1 Bessel Function

By inspection, we can find the spatial part of the solution. Which is an alternative form of the Sturm Liouville problem from subsection 5.2.2

$$\frac{\partial^2 R}{\partial r^2} + \frac{1}{r}\frac{\partial R}{\partial r} + \lambda^2 R = 0 \tag{7.18}$$

By adding $r^2$ to Equation 7.18 we can rewrite the equation and show that the Bessel function gives the general solution to the spatial problem.

$$R(r) = c_1 J_0(\lambda r) + c_2 Y_0(\lambda r) \tag{7.19}$$

The equation has two linearly independent solutions. Which are called the Bessel function of the first kind with zero order, $J_0(z)$, and Bessel function of the second kind with zero order, $Y_0(z)$. $J_0(z)$ solution is finite at $z = 0$ and $Y_0(z) \to \infty$ as $z \to 0$. To ensure that $R(r)$ is bounded, $|R(0)| < \infty$. We will let $c_2 = 0$ and $c_1 \neq 0$ only when $z = \lambda r$ is root of $J_0(z)$. Such that a non-zero solution can be found. The spatial solution will then reduces to.

$$R(r) = c_1 J_0(\lambda r) \tag{7.20}$$

The roots will have an infinite sequence of positive eigenvalues $\lambda_i > 0$ that would satisfy a stable solution to Equation 7.20. A numerical approximation of computing the eigenvalues are shown in section A.2. For notationally assurance, let the $i^{th}$ zero of $J_0(z)$ be defined as $\Gamma_i$. Hence, the corresponding $\lambda_i$ will be on the form of $\lambda_i = \Gamma_i/a$. Then, combining the solution with the Robin boundary condition yields the following relationship.

$$\begin{aligned} & L_c \lambda J_1(\lambda a) + \mathrm{Bi}\, J_0(\lambda a) = 0 \\ \Rightarrow\ & \mathrm{Bi}\, J_0(\Gamma_i) - \Gamma_i J_1(\Gamma_i) = 0 \end{aligned} \tag{7.21}$$

The Bessel function of the n'th kind is defined by a power series in the same way as the known trigonometric functions $sin(x)$ and $cos(x)$. The power series will converge for all $z \geq 0$ and uniformly for a closed interval $z \in [0, a]$. With convergence greater compared to the known exponential and trigonometric functions [48].

$$J_n(z) = \sum_{k=0} \frac{(-1)^k z^{2k+m}}{k!(k+m)!2^{2k+m}} \tag{7.22}$$

Although the trigonometric functions have exactly periodic properties, the Bessel functions are not uniformly periodic. However, it starts to show a periodic tendency for large values of $z$. This may be more apparent to see with the approximation of the power series.

$$J_n(z) \approx \sqrt{\frac{2}{\pi z}} \cos(z - [n/2 + 1/4]\pi) \tag{7.23}$$

The first 20 roots of the Robin boundary condition are plotted in Figure 7.2. It can be seen as scaled trigonometric functions, similar to the approximation of the Bessel function. The eigenvalues start to show a periodic tendency, and the amplitude increases.

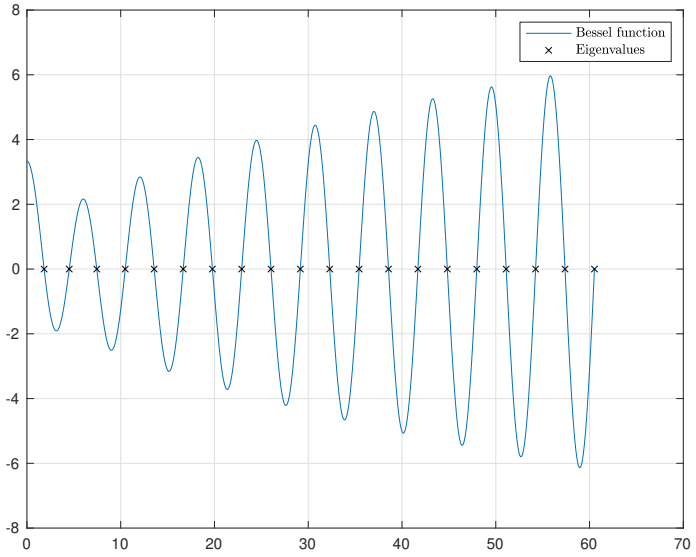


Figure 7.2: A plot of the Robin boundary with 20 corresponding eigenvalues.

We established in section 5.2: that an SLP can form a complete set on a closed domain $0 \leq r \leq a$, and the Gram-Schmidt orthogonalization can normalize an orthonormal set of eigenfunctions. Let the scaling coefficient $K$ form an orthonormal basis for the eigenfunction and be unit in the $\mathcal{L}_2([0, L], \mathbb{R})$ norm.

$$\sqrt{\int_0^a \left(J_0(\lambda r)\right)^2 r \, dr} = \sqrt{\int_0^a r J_0(\Gamma \frac{r}{a})^2 dr} = \sqrt{\frac{a^2 J_0(\Gamma)^2 + J_1(\Gamma)^2}{2}} \tag{7.24}$$

Let the scaling coefficient $K$ be the inverse of the solution of Equation 7.24.

$$K \triangleq \sqrt{\frac{2}{a^2 \left(J_0(\Gamma)^2 + J_1(\Gamma)^2\right)}} \tag{7.25}$$

Verify the choice of $K$ is normalized.

$$\sqrt{\int_0^a K J_0(\Gamma \frac{r}{a})^2 \, r dr} = 1 \tag{7.26}$$

We will show in section B.2 that the SLP is an orthogonal set of the eigenfunction, and a numerical evaluation can be seen in section B.3. We can then write the eigenfunction for the i'th mode as.

$$\phi_i(r) = \sqrt{\frac{2}{a^2 \left(J_0(\Gamma_i)^2 + J_1(\Gamma_i)^2\right)}} J_0(\lambda_i r) \tag{7.27}$$

### 7.2.2 Full Solution

Since the eigenfunctions are orthogonal, the SLP can form a complete set, in the same way as we previously established in subsection 5.2.4. Let the expansion coefficient be denoted as.

$$\tau_j = \int_0^a \phi_j \tau \; r dr \tag{7.28}$$

The PDE can be represented by an arbitrary accurate truncated sum.

$$\tau = \sum_{i=1}^{n} \phi_i \tau_i = \sum_{i=1}^{n} K_i J_0 \left(\lambda_i r\right) e^{-\alpha \lambda_i^2 t} \tag{7.29}$$

All told, the general solution for the linear homogeneous heat equation will be.

$$\tau(r,t) = \sum_{i=1}^{\infty} \int_0^a \phi_i(r) \phi_j \left(r'\right) e^{-\alpha \lambda_i^2 t} \tau \left(r', 0\right) r \; dr' \tag{7.30}$$

## 7.3 Weak Formulation

Let the eigenfunction be mapped to the global domain $\phi_i : [0, a] \to \mathbb{R}$ such that a weak form of the PDE can be established. If $\tau$ is a solution to the SLP, then the i'th modes for the eigenfunctions will fix the solution to zero, viz.

$$\int_0^a \phi_i \left( \frac{\partial \tau}{\partial t} - \alpha \frac{1}{r} \frac{\partial}{\partial r} \left( r \frac{\partial \tau}{\partial r} \right) \right) r \; dr = 0 \tag{7.31}$$

Integrating by parts is utilized on the spatial part of the equation, yielding a reformulation of the weak form.

$$\begin{aligned}
\int_0^a \phi_i \frac{\partial}{\partial r} \left( r \frac{\partial \tau}{\partial r} \right) dr &= \alpha \left[ \phi_i r \frac{\partial \tau}{\partial r} \right]_0^a - \alpha \int_0^a \frac{\partial \phi_i}{\partial r} r \frac{\partial \tau}{\partial r} \; dr \\
&= \alpha \left[ r \left( \phi_i \frac{\partial \tau}{\partial r} - \tau \frac{\partial \phi_i}{\partial r} \right) \right]_0^a + \alpha \int_0^a \tau \frac{1}{r} \frac{\partial}{\partial r} \left( r \frac{\partial \phi_i}{\partial r} \right) r \; dr \\
&= \alpha \left[ r \left( \phi_i \frac{\partial \tau}{\partial r} - \tau \frac{\partial \phi_i}{\partial r} \right) \right]_0^a + \alpha \int_0^a \tau \left( \frac{1}{r} \frac{\partial \phi_i}{\partial r} + \frac{\partial^2 \phi_i}{\partial r^2} \right) r \; dr \\
&= \alpha \left[ r \left( \phi_i \frac{\partial \tau}{\partial r} - \tau \frac{\partial \phi_i}{\partial r} \right) \right]_0^a - \alpha \int_0^a \tau \left( \lambda_i^2 \phi_i \right) r \; dr
\end{aligned} \tag{7.32}$$

In the same way as section 5.3, the reformulated spatial part of the integral naturally produces the Robin boundary condition. We use the eigenfunction

properties to simplify the weak form and insert the reformulation into the generalized solution, yielding.

$$\int_0^a \phi_i \left( \frac{\partial \tau}{\partial t} + \alpha \lambda_i^2 \tau \right) r \, dr = \alpha \left[ r \left( \tau \frac{\partial \phi_i}{\partial r} - \phi_i \frac{\partial \tau}{\partial r} \right) \right]_0^a \tag{7.33}$$

The eigenfunctions ensure that the homogeneous boundary conditions are upheld at the surface. Thus, we can deduce that temperature at the boundary can be written as.

$$\begin{aligned} \left[ r \left( \phi_i \frac{\partial \tau}{\partial r} - \tau \frac{\partial \phi_i}{\partial r} \right) \right]_0^a &= \left( a \left( \phi_i \right)_a \left( \frac{\partial \tau}{\partial r} \right)_a - a \tau_a \left( \frac{\partial \phi_i}{\partial r} \right)_a \right) - 0 \\ &= - \left( \phi_i \right)_a \left( a \left( \frac{\partial \tau}{\partial r} \right)_a + \mathrm{Bi} \, \tau_a \right) \\ &= \left( \phi_i \right)_a \left( \mathrm{Bi} \, u + \frac{a}{k} v \right) \end{aligned} \tag{7.34}$$

Inserting the solution from Equation 7.34 into Equation 7.33 will yield a reduced weak form of the SLP.

$$\int_0^a \phi_i \left( \frac{\partial \tau}{\partial t} + \alpha \lambda^2 \tau \right) r \, dr = \left( \phi_i \right)_a \frac{\alpha}{L} \left( \mathrm{Bi} u + \frac{a}{k} v \right) \tag{7.35}$$

Denoting $b_i$, for later use.

$$b_i \triangleq \left( \phi_i \right)_a = \sqrt{\frac{2}{a^2 \left( J_0(\lambda_i a)^2 + J_1(\lambda_i a)^2 \right)}} J_0(\lambda_i a) \tag{7.36}$$

## 7.4 Discretization

The model expansion for $\tau$ is inserted into the weak form, and a decoupled system of ODE's can be solved. Note that the eigenfunctions are orthonormal to each other.

$$\frac{\partial \tau_j}{\partial t} + \alpha \lambda_j^2 \tau_j = b_i \alpha \left( \mathrm{Bi} \, u + \frac{a}{k} v \right) \tag{7.37}$$

With a state vector for the i'th mode denoted as.

$$\boldsymbol{\tau} \triangleq \begin{bmatrix} \tau_1 \\ \tau_2 \\ \vdots \\ \tau_i \end{bmatrix} \tag{7.38}$$

Let $\mathbf{\Lambda}_{ii} = -\alpha \lambda_i^2$ be a diagonal matrix for each mode. Also, define $\mathbf{b}$ as an vector, which holds the $b_i$ values for the i'th mode.

$$\dot{\boldsymbol{\tau}}(t) = \boldsymbol{\Lambda}\boldsymbol{\tau}(t) + \boldsymbol{b}\alpha\left(\mathrm{Bi}u(t) + \frac{a}{k}v(t)\right) \tag{7.39}$$

Using the eigenfunctions, an output for the model can be found at $r = r_m$.

$$y(t) = \sum_{i=1}^{n} \phi_i\left(r_m\right)\tau_i(t) = \boldsymbol{c}\boldsymbol{\tau}(t), \quad c_i = \phi_i(x) \tag{7.40}$$

# 8 | Experimental Setup

Two experiments were conducted to validate the two-dimensional spectral model. The result from the experiment was used to ascertain the thermal properties constants and compared against the model.

## 8.1 Overview of the setup

The test consisted of two different beef types, a round steak and a tenderloin acquired at the local butcher. The two types of cuts were chosen with a length greater than the diameter of the cut. As a consequence of the assumption in the model: *The convective/radiative heat source is larger over the radial surface to the vertical surface.* The samples have a naturally cylindrical form and, prior to cooking, were bound up with butchers twine or pre-assembled with a netting. Making the sample almost uniform, and the assumption of angular symmetry can be imposed. Both cuts have a moderate amount of marbling throughout the fibres, and any superficial connective tissue was removed. It can be noted that the round steak has more connective tissue throughout the fibres, which make it tougher/chewier. Compared to the tenderloin.

The experiment was carried out with the following step:

- The circumference, length and weight of the meat were measured, and the radius and density were calculated. Seen in Table 8.1
- The meat was equipped with two thermal sensors at $r = 0$ and $r = R/2$, and one control sensor at $r = R/2$. As seen in Figure 8.3 and Figure 8.4.
- The oven was preheated with the free convection setting, and when the oven showed a steady-state temperature of $250°C$. The samples were laid in the central region of the oven on an oven rack. Assuming an even temperature distribution around the cut is produced. The round steak sample was exposed to only free convection, and the tenderloin was first exposed to free and then switched to forced convection.
- Temperature telemetry was logged every two minutes inside and outside of the meat, And the logging can be seen in Appendix C. The cooking process was assumed finished when the thermal sensors at $\tau(R/2, t)$ read $52°C$ and removed from the oven.
- The thermophysical properties were estimated via two methods. The first was done with manually parameter estimation. Secondly, using the

mean values from telemetry readings and using the linearized function and composition data from section 3.5.

| Description | Value | Unit |
|---|---|---|
| Initial temperature | 8 | $°C$ |
| Initial weight | 1.131 | $[kg]$ |
| Final weight | 0.933 | $[kg]$ |
| Circumference | 295 | $[mm]$ |
| Length | 160 | $[mm]$ |
| Calculated radius | 47 | $[mm]$ |
| Calculated density | 967 | $[\frac{kg}{m^3}]$ |

(a) Round steak

| Description | Value | Unit |
|---|---|---|
| Initial temperature | 17 | $°C$ |
| Initial weight | 0.819 | $[kg]$ |
| Final weight | 0.644 | $[kg]$ |
| Circumference | 250 | $[mm]$ |
| Length | 170 | $[mm]$ |
| Calculated radius | 39.8 | $[mm]$ |
| Calculated density | 1.027 | $[\frac{kg}{m^3}]$ |

(b) Tenderloin

Table 8.1: Parameter values from the experiment

### 8.1.1 Thermal Sensor

The thermal sensor used for the experiment where a commercially available sensor named Meater® [49]. The Meater sensor was selected because it has two built-in sensors, see Figure 8.1. The first sensor measures the temperature internally and is located 2cm from the tip. The second sensor is external, measuring the ambient temperature, approximately 2-4 cm outside the surface of the meat. The thermal sensor sends the temperature data via Bluetooth 4.0 to an external device.


Figure 8.1: A sketch of the placement of the different sensors [50].

There is no available technical specification document on which type of sensor used in the Meater product. Only a limited specification for the characteristics is given on Meater's official website [51]. The relevant specification for this experiment is listed below.

- Maximum internal temperature: $212°F \approx 100°C$
- Maximum ambient temperature: $527°F \approx 275°C$
- Variance internal sensor: $\pm 0.5°C$

The control sensor was a built-in sensor in the domestic oven and was used to validate the result from the Meater sensor. The domestic oven was of the bran *Bosch Serie-8 Oven*. The documentation for the oven does not state which type of sensor used or the variance of the sensor. The relevant data found for this experiment was; the thermometer worked in the range of $\tau(x,t) \in [30, 99]°C$

[52]. The reading was discarded due to the limitation of the probe and are not include henceforth.

### 8.1.2 Time Delay in the Ambient Sensor

The telemetry from the ambient sensor showed a significant time delay when exposed to a high heat source. As a consequence, the time delay for the ambient sensor is needed. If we assume the ambient temperature reading is correct and have the characteristic of a low-pass filter. The ambient telemetry can be stated on the form.

$$\zeta \dot{\tilde{T}}(t) + \tilde{T}(t) = T_0 \tag{8.1}$$

Here, $\zeta$ is denoted as the time constant, $\tilde{T}(t)$ is a measurement at time $t$, and $T_0$ is the constant temperature in the oven. Note that we neglect the thermal cycling from the oven. The equation can readily be solved with.

$$\tilde{T}(t) = T_0 + (\tilde{T}(0) - T_0)e^{-t/\zeta} \tag{8.2}$$

The time constant $\zeta$ can be found by solving the low-pass filter, viz.

$$\zeta = -\frac{t}{ln\left(\frac{T_0 - \tilde{T}(t)}{T_0 - \tilde{T}(0)}\right)} \tag{8.3}$$

Two different Meater sensors were used, and the telemetry from the sensor produced a time constant of $\zeta_1 = 98.3$ and $\zeta_2 = 103.8$ seconds. Assuming $T_0 = 5 \cdot \zeta$ gives steady-state temperature readings. Telemetry readings after approximately 9 min can be used as the steady-state temperature for $t = 0$. A simplification can be done by setting the mean value of the sensor to be the controller input $u(t)$.

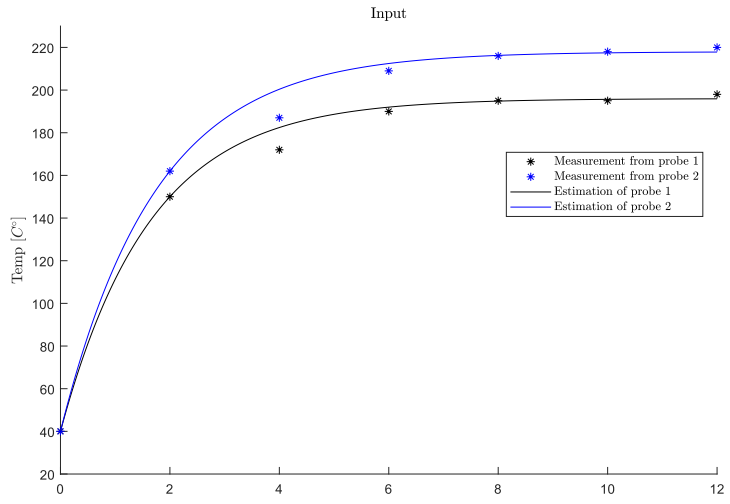


Figure 8.2: A low pass filter estimating the time constant.

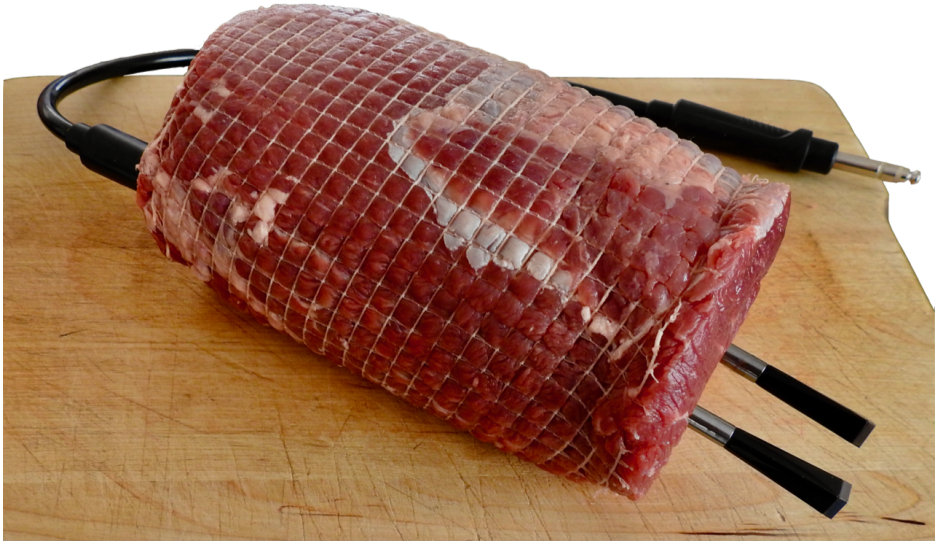

Figure 8.3: The round steak sample. With three thermal sensors insert.

Figure 8.4: The tenderloin sample. With two thermal sensors insert.

# 9 | Result and Discussion

## 9.1 Experiment

The experiment was done without a simulation first. To facilitate how two amateur home cooks used intuition and their knowledge of thermodynamics to assert when the meat was finished. We came to a conclusion that if the thermometer at $\tau(R/2, t) = 52°C$. The residual heat would propagate from the boundaries, and an idealized steady-state temperature of $\tau(r, t) \approx 55°C$ could be accomplished.

### 9.1.1 The Round Steak Sample

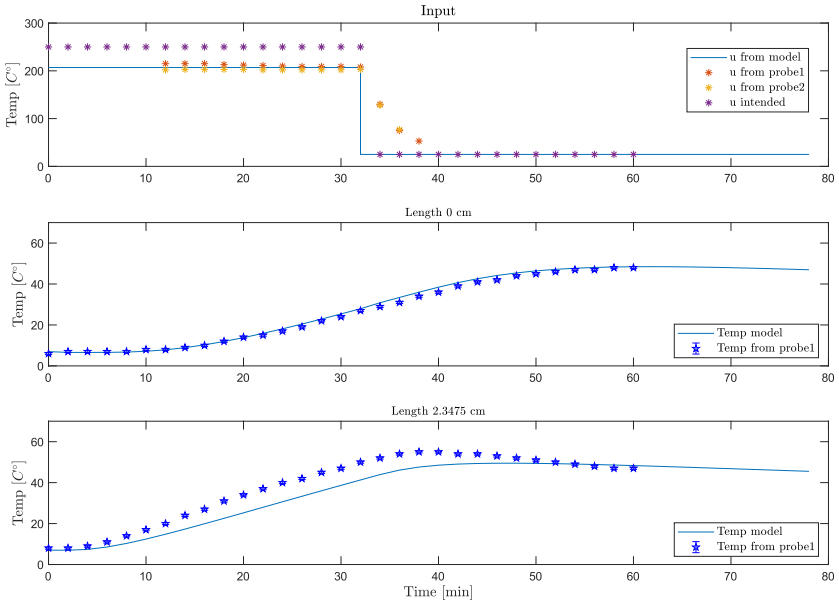


Figure 9.1: Telemetry data for the round steak compared to the spectral model. Done with manually parameter estimation.

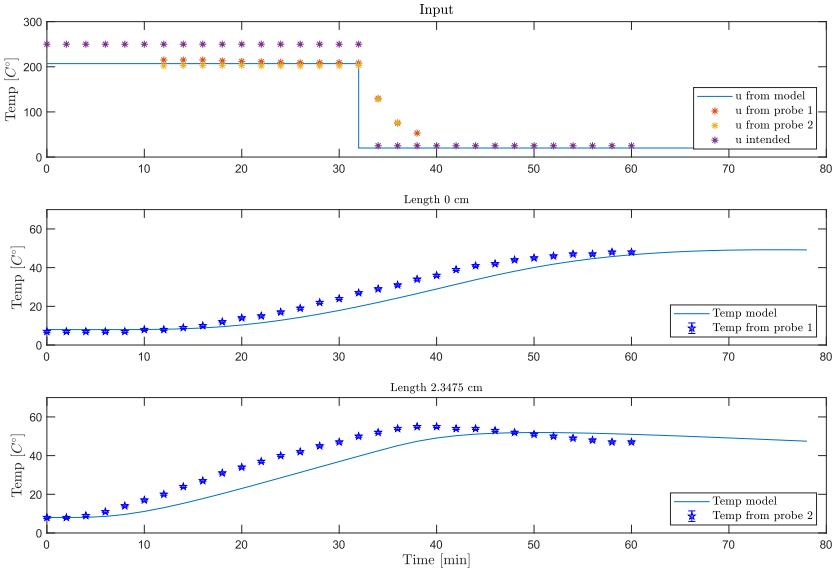


Figure 9.2: Telemetry data for the round steak compared to the spectral model. Done with composition data.

Figure 9.1 and Figure 9.2 shows the sequential logged values from the experiment, which are plotted against the two-dimensional cylindrical spectral model. Where the round steak sample was exposed to the free convection setting, with a temperature input set to $u_{oven} = 250°C$. Both the Meater sensor was located on the same side of the roast. Even if they were closely spaced. The ambient temperature telemetry varied in range of $[2, 13]°C$ and gave a negative temperature difference of $[35, 47]°C$ compared to $u_{oven}$. Seen in the top part of Figure 9.1 and Figure 9.2. We will, therefore, consider a mean value of the ambient telemetry as the input for the spectral heat equation. With the assumption that a time delay of 9 minutes gives steady-state temperature. The calculated mean value is therefore set to $u_{mean} = 207°C$ for $\tau(r, t) \in [0, 32)$. The roast was removed from the oven and exposed to the ambient room temperature of $u_{amb} = 25°C$. Which will produce the following step response for the model.

$$u(t) = \begin{cases} u_{mean} & t \leq 32 \\ u_{amb} & t > 32 \end{cases} \tag{9.1}$$

Thermophysical properties via manually parameter estimation produced a Biot number of $\text{Bi} = 0.8$ and thermal diffusivity of $\alpha = 2.28e - 7$. Secondly, the estimated thermophysical properties with composition data, found a thermal diffusivity of $\alpha = 1.33e - 7$ and thermal conductivity of $k = 0.5$. Assuming a heat transfer coefficient of $h = 20$ produced a Biot number of $\text{Bi} = 1.9$.

Figure 9.1 are fitted with parameter estimation, and we can observe that the model tracks the core temperature within a small tolerance. The sensor placed at $\tau(R/2, t)$ deviates from the steepest gradients compared to the spectral model. However, after $t = 50$ $[min]$, the model and the telemetry data starts to consolidate. Figure 9.2 uses the estimated thermophysical properties and

shows a similar thermal characteristics. By using the estimated quantities, a larger deviance from the model to the actual data-set occurred for both $\tau(0,t)$ and $\tau(R/2,t)$.

Both Figure 9.1 and Figure 9.2 shows that thermal energy builds up faster at $\tau(R/2,t)$ compared to $\tau(0,t)$. This is consistent with what we have seen in previous simulation of the heat equation. Latent heat propagates into the meat after the sample is taken out of the oven. Where it takes longer time to dissipate the residual heat for the centre compared to $\tau(R/2,t)$. With the temperature reaching a steady-state at $t = 60$ $[min]$ and $\tau(0) = 48°C$ and $\tau(R/2) = 47°C$. Which means that accounting for a variance of $\pm 0.5°C$ in the internal temperature sensor, the temperature should not be any higher in the core due to the maximum principle. This entails that the meat will not exceed a temperature of $48°C$ and $\tau(r,t) = 55°C$ are not obtained.

### 9.1.2 The Tenderloin Sample

The tenderloin sample was first subjected to free convection and switch to the forced convection setting, with $u_{oven} = 250°C$. The switch occurred at $t = 14$ $[min]$ and removed at $t = 24$ $[min]$. Additionally, the Meater sensor was inserted on the opposite side to each other. These alterations were done to understand if the thermophysical properties were affected by the placement of the sensor and sudden changes in convection.

from Figure 9.3 and Figure 9.4. We can observe that while the forced convection setting was applied, the temperature spiked about $20°C$. This is no surprise since the fan will push the heated air over the boundaries of the meat and the ambient sensor. However, with the sensor on the opposite side of each other, we get an ambient temperature difference between the sensor of $[21, 23]°C$ under free convection and $[13, 15]°C$ for forced convection. Which is larger compared to the previous experiment. The same procedure as the round steak was used and produced a mean value for the input to $u_{mean,free} = 208°C$ and $u_{mean,forced} = 234°C$.

$$u(t) = \begin{cases} u_{mean,free} & t \leq 14 \\ u_{mean,forced} & 14 < t \leq 24 \\ u_{amb} & t > 24 \end{cases} \tag{9.2}$$

Figure 9.3 are manually parameter estimated and the following values was found: $\alpha = 2.04e-7$ and $\text{Bi} = 0.8$. Whereas, Figure 9.4 are estimated with composition data, producing a: $\alpha = 1.31e-7$ and $\text{Bi} = 1.8$. We can observe that the Biot number and the thermal diffusivity constant is relative the same for the tenderloin and the round steak with both methods.

From Figure 9.4 and Figure 9.4, we can observe the concavity for $\tau(0,t)$ and $\tau(R/2,t)$. Are almost identical to the telemetry data, even with different thermophysical values. The parameter estimated quantities showed the best result with the spectral model. We can additionally see temperature propagation after the meat was taken out of the oven, at $t = 24$ $[min]$. Resid-

ual heat propagates to the core, and at half the radius of the meat. With steady-sate temperature occurring at $t = 46$ $[min]$ and $\tau(0,t) = 55°C$ and $\tau(R/2,t) = 55°C$.

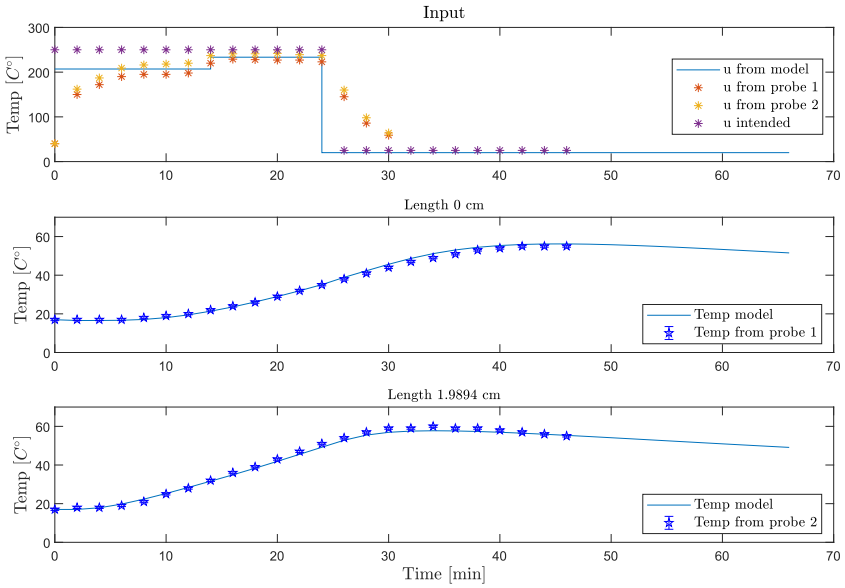


Figure 9.3: Telemetry data for the tenderloin compared to the spectral model. Done with parameter estimation

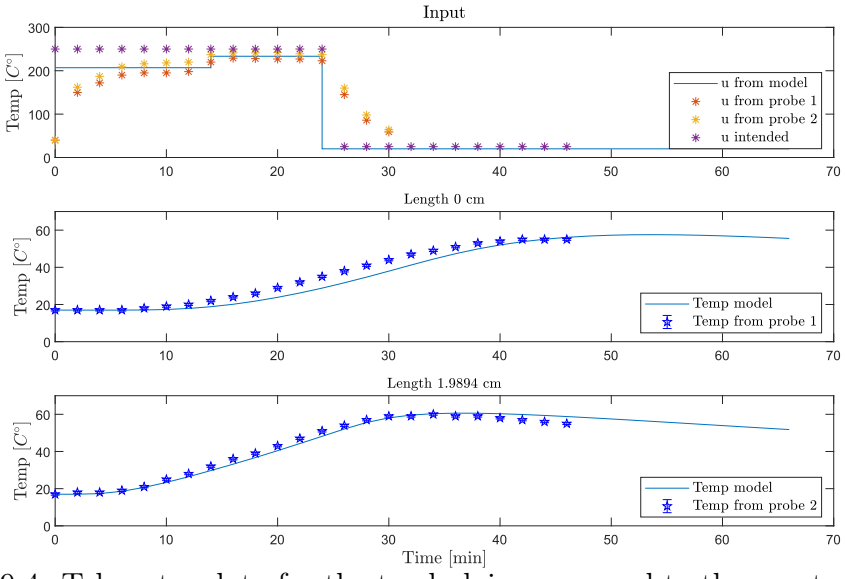


Figure 9.4: Telemetry data for the tenderloin compared to the spectral model. Done with composition data.

### 9.1.3 General Discussion

The two-dimensional spectral method provides a surprisingly good results for the tenderloin sample. This cut had the least cylindrical shape. Prior to the analysis, the round steak was expected to give the best result due to the cylindrical homogeneity of the sample. This is an interesting finding, and it could be hypothesized that a larger ratio of circumference to length could be a reason

for these findings. One of the model's fundamental assumptions is that heats enter through the radial surface. When spontaneous heat transfer via convection occurs at the boundaries. Thermal energy is diffused via conductivity into the meat. Since beef consists of approximately 70 - 75 % water, evaporation at the boundaries will occur. Considering that mass transfer of meat juices occurs at the boundary, the beef starts to shrink when heat is applied. However, the relative ratio is approximately alike. The cylindrical homogeneity of the round steak could be somewhat deceiving. In hindsight, it would make sense that the model is better to approximate the tenderloin sample. The convective heat source pushes more thermal energy into the vertical surface of the round steak compared to the tenderloin. We can see that the assumption of angular symmetry is justified and does not affect the modelling error significantly. Further investigation to improve on these new developments is suggested by accounting for the vertical surface.

Furthermore, the evaporation of meat juices on the boundary can have an additional effect on the model. It can create an insulating layer around the steaks, such that less heat flux enters the system. This makes the Neumann condition the significant contributory factor in the Robin boundary condition. It was observed a difference of up to $47°C$ from the ambient sensor and the oven setting. An important factor in the model is that the input matrix is model as the thermal energy at the boundary. If the reading from the oven does not correlate with the temperature at the boundary. A significant model mismatch could occur. This shows the importance of a temperature sensor close to the meat for this model.

With various assumption in the model, some deviation was expected. The thermophysical properties found in literature research, and parameter estimated were close to each other but not conclusive. With the spectral model showing the best approximation for the tenderloin sample. Both with conventional and estimated values. In section 3.5 the thermophysical properties were estimated with a mass fraction and general composition data. Gathering a sufficient amount of data can be a complex process, and the amount of water, fat and protein was not measured for both samples. This most likely causes the round steak to give a poorer estimate with the composition data. Given the circumstances can thus be considered reasonably successful for the round steak. However, curve fitting produces better quality in the results. We can observe that the dimensionless Biot number was the same for both samples, even if they were exposed to free or forced convection. This makes the use of a dimensionless Biot number a vital asset for the model. This implies that a generalized Biot number can be found and should be considered in future experiments. The thermal conductivity coefficient is not as easy to generalize. It describes the thermal inertia of an object. However, we can see that both samples had a similar thermal characteristic for both instances. It may be helpful to study particular aspects of thermal properties regarding the proposed model in future work.

Since the experiment participants did not want any food waste, the meat had to be consumed when the target temperature was reached, and the experiment was concluded. The assumption of $\tau(R/2, t) = 52°C$ produced an even temperature for about 75-80 % of the circumference of the tenderloin. It was pink in the centre, and approximately 1 cm of the outer edges showed tanning. Which entails that the tenderizing point at the edge of the steak had become deactivated. However, it was juicy and tender. The round steak did not reach the right core temperature and was placed in a sous vide and stored for later consumption.

## 9.2 Model-Based Roasting Control

The results suggest that the model is promising and can be used with an MPC, especially if we used the parameter estimated values for the tenderloin. In a real-life application, a reasonable assumption is that only one sensor would be used. This could be inserted at the core, and the spectral model can facilitate the rest of the unknown measurements. Constraints can be added to the MPC, and an idealized temperature profile can be found. We will consider two scenario, the first is an even temperature distribution $\tau(r, t) = 55°C$. The second will allow tenderness to decrease by 15% inside the circumference. Similarly to what we showed in section 6.2. The second simulations are done to see if we can shorten the time to cook the meat and restrict the meat denaturation. Such that unwanted irreversible changes do not occur.

### 9.2.1 Scenario 1: Even Temperature Distribution

We will aim to get the temperature distribution of a simulated tenderloin to be medium doneness, i.e. $\tau_{med} \triangleq 55°C$. As mention in section 2.3 water reduction occurs at $\tau(r, t) > 60°C$ and medium doneness is in the domain of $\tau(r, t) \in [55, 60]°C$. The tenderness of a beef decreases for $\tau(r, t) > 65°C$ and above $\tau(r, t) \in [70, 80]°C$ the tenderizing point deactivates. However we do not allow the tenderizing point to become deactivate and assume that occurs at $\tau_{max} \triangleq 70°C$.

The single input multi-output system will be consider for the measurement $\boldsymbol{y_k} = [R_0 \quad R_{0.5} \quad R_{0.9} \quad R]^T$. I.e. at the centre, 50 % from the centre, 90 % from the centre and the circumference. With the penalty matrices, $\mathcal{Q} = diag([4 \quad 4 \quad 4 \quad 80])\beta$ and $\mathcal{R}_{\Delta u} = 0.1/\beta$. Where the overall adjustment factor $\beta = 1.7$. The model can be fitted with more constraints to the measurement. However, there is only a single input to multiple outputs, and excess degrees of freedom are not available. It was detected that four constraints were sufficient to produce a good result when tuning the controller. The following constraints and quantities are listed up in Table 9.1.

| Symbol | Variable | Value | Unit |
|---|---|---|---|
| R | Radius | 4 | $[cm]$ |
| $\alpha$ | Thermal diffusivity | $2.04e-7$ | $[m^2/s]$ |
| Bi | Biot number | 0.8 | $[-]$ |
| $r_k$ | Reference variable | 55 | $[°C]$ |
| $x_0$ | Initial temp. distribution | 20 | $[°C]$ |
| $u_{k-1}$ | Last move of the input | 225 | $[°C]$ |
| $y_k^{\text{low}}, y_k^{\text{high}}$ | Min & max temp. to OV | $[20, 55]$ | $[°C]$ |
| $u_k^{\text{low}}, u_k^{\text{high}}$ | Min & max temp. to MV | $[20, 225]$ | $[°C]$ |
| $\Delta u_k^{\text{low}}, \Delta u_k^{\text{high}}$ | Min & max temp. rate to MV | $[-0.25, 0.5]$ | $\left[\frac{°C}{s}\right]$ |

Table 9.1: Parameter values for a simulated tenderloin steak.

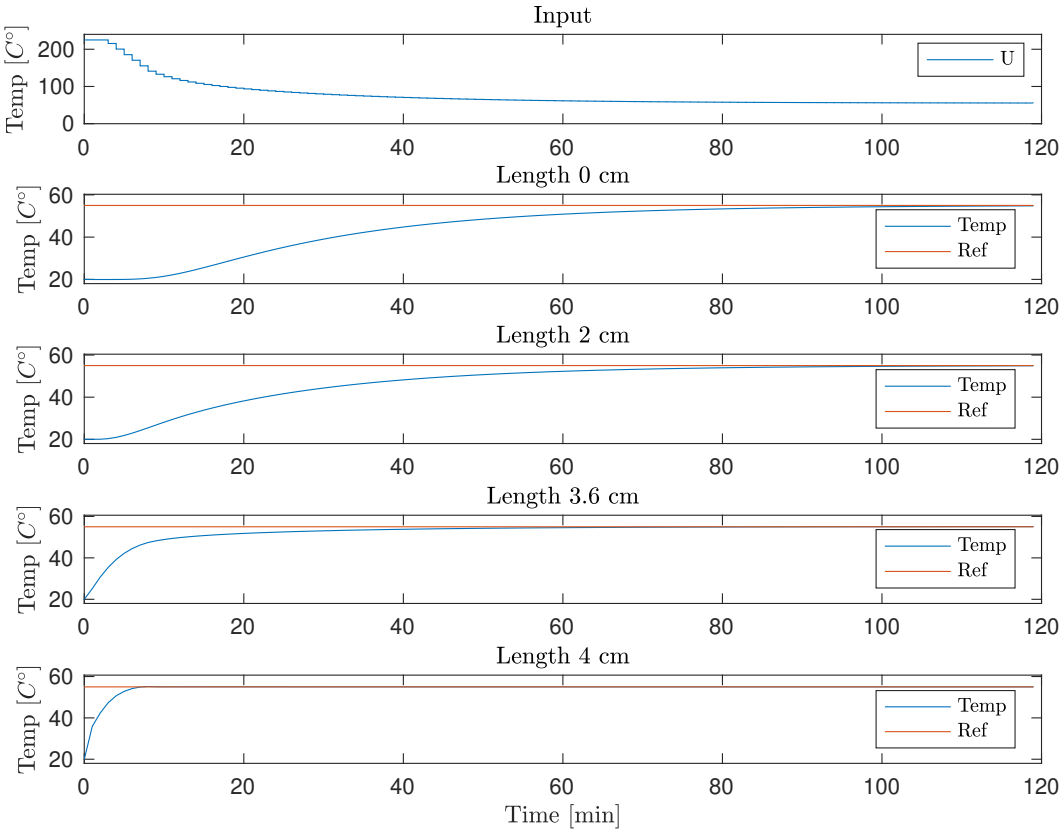


Figure 9.5: A cross-section of the four different measurements, with the controller input. For a tenderloin steak being simulated to ideally medium doneness.

From Figure 9.5 one can see that the input holds $y_k^{\text{high}}$ for approximately 4 minutes. The input starts to smooth out after the initial jolt of high temperature to an equilibrium of $55°C$ at $t \approx 100$ $[min]$. Since we start the simulated temperature at the edge of the active set, we introduce a slack variable to the measurements and the constraints. This will ensure that any unexpected temperature differences are not outside the feasible set. We can further observe that the measurement is inside the constraints, with a relatively high cost to the reference at the circumference. The steady-state temperatures, $\tau_{med}$, oc-

curs at $t \approx 110$ $[min]$, and it can be noted that this method does not exceed $\tau(r,t) \in [55,60]^{\circ}C$. Theoretically, no tenderness decrease occurs for the entire simulated steak.

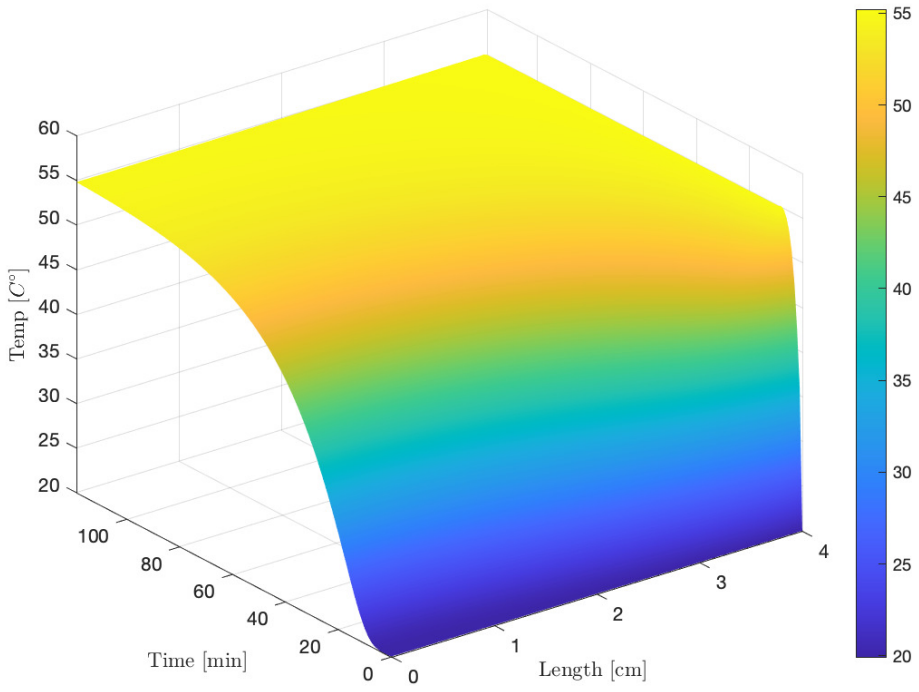


Figure 9.6: A 3d visualization where 0 is the centre of the disk and 4 is at the circumference. For a tenderloin steak being simulated to ideally medium doneness.

### 9.2.2 MPC Scenario 2: Irregular Temperature Distribution

We will consider the same parameters values from Table 9.1 and measurements. With an altercation to the reference variable, the constraint $y_k^{\text{high}} = 70^{\circ}C$ and the penalty matrices $\mathcal{Q} = diag([4 \quad 4 \quad 16 \quad 8])\beta$ and $\mathcal{R}_{\Delta u} = 0.1/\beta$. With $\beta = 1.7$.

$$r_{k+i} = \begin{cases} \tau_{med} & \text{if} \quad R_0 \leq x_k \leq R_{0.85} \\ \tau_{med} + b \cdot \tau_{max} & \text{if} \quad x_k > R_{0.85} \end{cases} \tag{9.3}$$

Where $b$ are a scaling coefficients for $t \in [0, i/2]$.

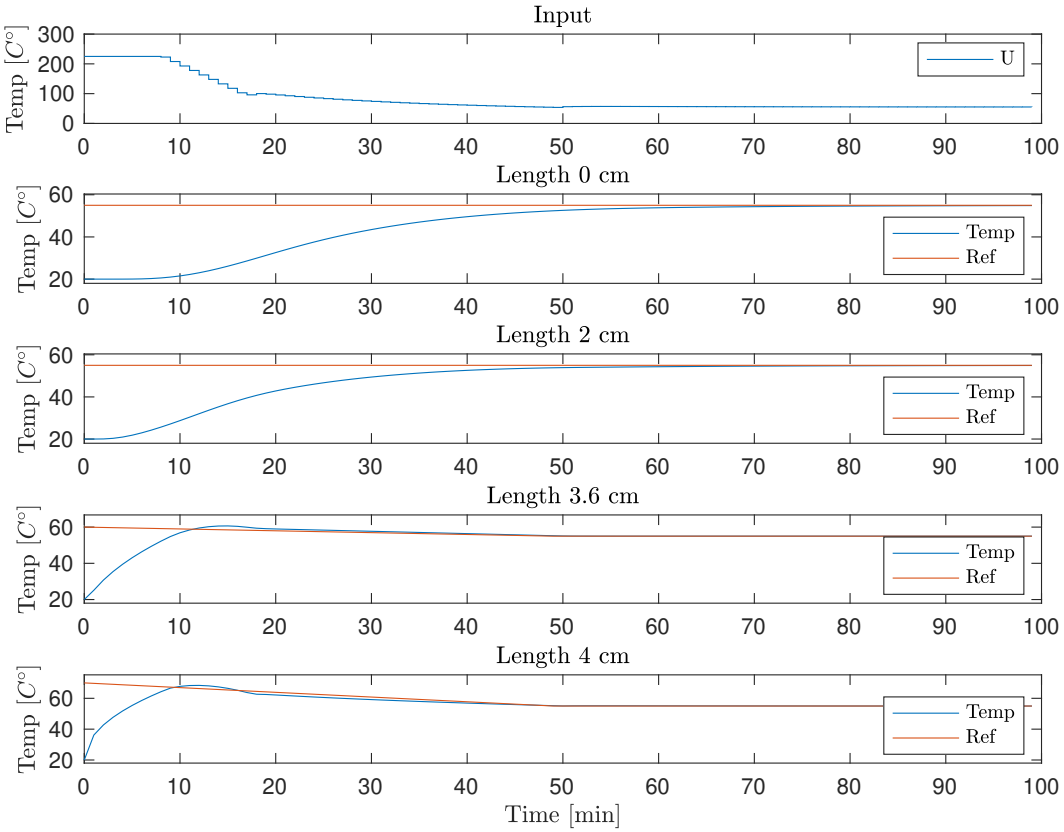


Figure 9.7: A cross-section of the four different measurements, with the controller input. For a tenderloin steak being simulated to nearly ideally medium doneness.

One noticeable difference from the previous scenario. Is that we have a larger overshoot to the circumference of the simulated tenderloin, as seen in Figure 9.7. The temperature at the peak is approximately 68.5°$C$ at the circumference, which makes the tenderness decrease. However, the tenderness does not become deactivated since we chose the reference tracking vector to vary in time. The MPC corrects the overshoot area steadily down to $\tau_{med}$. Another notable difference is that the penalty matrices are more tune in favour of the third measurement, i.e. $R_{0.9}$. Which gave a slight overshoot with a temperature peak of 60°$C$, and are bordering on the medium doneness domain. This manifest as the spike in Figure 9.8. We can also observe that the maximum allowed temperature input is held for a longer time than the previous simulation. However, we produce the same temperatures characteristic for the input, except for some minor correction. With these minor adjustment to the reference tracking vector and allow some decrease in juiciness, a steady-state temperature of $\tau_{med}$, can be reached at $t \approx 70$ $[min]$ for 80% of the meat.

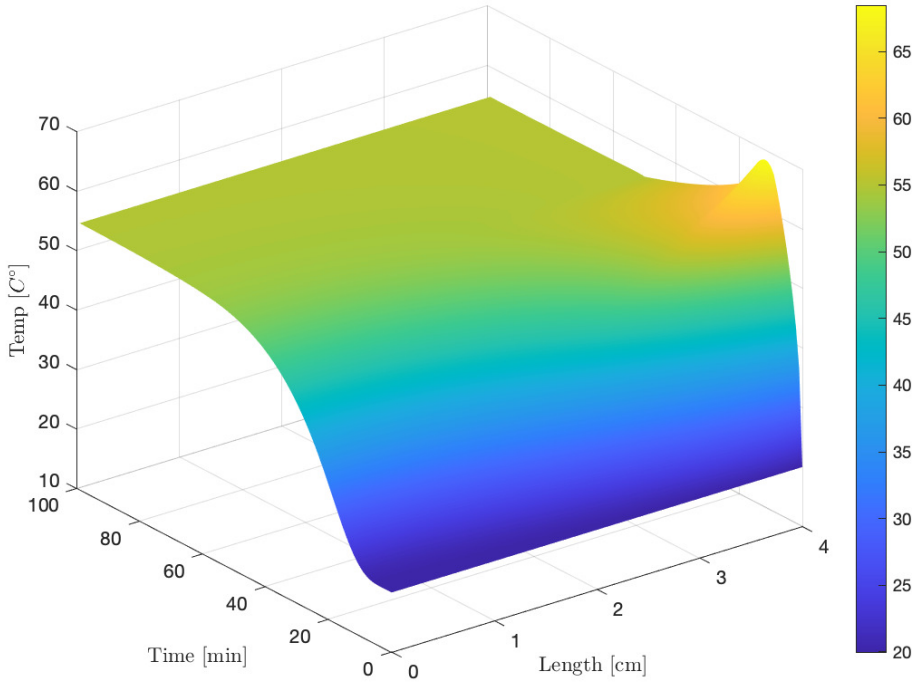


Figure 9.8: A 3d visualization where 0 is the centre of the disk and 4 is at the circumference. For a tenderloin steak being simulated to nearly ideally medium doneness.

### 9.2.3 General Discussion

The findings from the results show a quite interesting controller input profile. Recall from section 1.1:*Perfectly roasted meat are often exposed to high heat first, then roasted at a lower heat setting.* The MPC strategy produced the same result in a natural way. This comes from how the MPC interact with the heat equation and are bounded by the thermophysical properties. The results suggest that an MPC was able to forecast the thermodynamics properties of the tenderloin, and it may be possible to control a steak to the desired temperature profile. However, this is an idealized scenario. The main focus of this thesis was to see if it was possible to use an MPC with an analytical thermodynamic model, and we would recommend in future studies that disturbance and measurement noise are accounted for with a state estimator or empirical studies.

The application of this system may show an increased result in temperature evenness when roasting a steak. We observe that both simulated scenarios gave no tenderness deactivation to the simulated tenderloin. The first scenario produced an even temperature distribution over the entire domain. Since we optimize for temporal properties and not the transit behaviour, the cost is a lengthy time to reach medium doneness. The second scenario sacrificed tenderness for 10% of the radius and took 40 minutes shorter to reach an even temperature profile of medium doneness. However, beef with more connective

tissues would need the sarcoplasmic proteins to be activated via slow cooking below $60°C$. Cuts with long sarcomere fibres due to the hanging process post mortem have a total roasting time proportionally to the cut of the meat. For example, a temperature model for cuts of meat with short sarcomere fibres needs to take into account the time needed to tenderize the meat, i.e. long roasting periods at low temperatures. This is not accounted for in the MPC algorithm. However, the first model showed that we never breached the constraints and $\tau(r,t) < 60°C$ and the meat could be further roasted after the steady-state temperature was found.

Furthermore, we can observe that the strategy we found in section 6.2 of starting at high temperature is feasible due to the low Biot number. However, the model is not limited to be used in ovens. The model-based roasting controller may be applied in sous vide, barbeques and steam jet injection oven, to mention a few application. We tested the model vigorously with relative high Biot's numbers in section 5.5, and from the table in subsection 3.5.2. Water and steam have a higher convection coefficient, which implies that the Biot number would increase and we might have to initiate the MPC at a lower temperature.

When adding constraints to the MPC, several factors had to be considered. There is no definite answer if the meat should be rare, medium or well done, which will be up to the individual consumer's. The constraints are based on the eating quality research found in section 2.2 and the effect of thermal energy on a steak in section 2.3: Tenderness, juiciness, reduced-fat and water loss, colouring and beef flavour. The beef flavour is taken into account with the initial high temperature in the model (above $140 - 160°C$) which may create the Maillard effect. The gradual reduction in temperature and the slow roasting methods are based on research showing that the cooking quality increases with a more extended roasting period. Furthermore, the model may reduce the risk for undercooked meat, with increased risk for pathogens in the meat, and charred steak with a higher concentration of heterocyclic amines, thus higher risk for cancer. As discussed in section 2.4.

The model-based roasting controller can adjust the constraints to satisfy the preferred doneness of an individual consumer. If the model-based roasting controller were to be deployed. The consumer could select the preferred doneness, and the constraints could be updated based on different doneness-simulation and types of meat. The system could be run in an open-loop or closed-loop configuration, where the open-loop system could be used in conjunction with a household thermometer. Inserted in the core of the meat, and the model can calculate the auxiliary measurement. This can be paired with an application program interface (API) interfaced with a remote server. The MPC algorithm can be calculated on the server and send the control sequence and re-optimised for a discrete-time step. The consumer can then adjust the temperature setting manually, e.g. 1-5 minutes.

However, the MPC can be susceptible to model mismatch in the plant. We observed that a relative professional domestic oven did not reach the set tem-

perature setting around the steak. This means that using the input reading from the heat source could give false controller input. Additionally, the quantities for the manipulated variable will be needed for the specific oven. In the simulation, we assumed that heat dissipated at half the rate it gains heat; this will vary from oven to oven. This again shows the importance of temperature measurements near the steak. A thermometer with an internal and ambient sensor, like the Meater probe, could be used. It could run preliminary tests in an oven, find the rate of changes, and update the parameters back to the server. That way, we are more likely to achieve a better result. If the system were in a closed-loop configuration, it would be reasonable to assume the model-based roasting controller would perform in a better capacity. A domestic oven can be integrated with a thermal sensor and the proposed method. A remote server or an internal computer can calculate the optimized controller input and regulate the heat source. Further investigation is necessary to see if using the model-based controller in a live application is possible.

# 10 | Conclusion

This thesis aimed to explore if a mathematical model of the heat equation could use the benefits from an MPC to achieve an idealized temperature profile for a steak. This was first approached by modelling the heat equation in one dimension and exploring two different models. The finite-difference approximation of the laplacian showed promising results in modelling the thermodynamics of a roast. However, the finite difference method only approximated its nearest neighbour's stencil. This meant that expanding the grid size for an increasing time domain and spatial dimension became computationally expensive. The spectral method has a high spatial resolution for a long integration time since it seeks a global solution to the heat equation. Although, it is intricate to solve. We achieved a more robust method, and mathematical analysis ensured a stable solution for the heat equation. The outcome of various simulation for both methods lead to the conclusion that the spectral method had the highest overall robustness and performance.

The spectral method was extended into cylindrical coordinates and validated against two different types of steaks. The result from the experiment showed that the two-dimensional spectral model approximates the roasts' thermal dynamics well, where the tenderloin sample had the best thermal characteristic. This led to the conclusion that one thermal sensor could be inserted in the meat's core, and the spectral model could facilitate the rest of the unknown measurement. Several simulations of the heat equation with an MPC showed a promising result of achieving an even temperature profile throughout the meat. With an interesting input profile, of starting at a high initial temperature and a steadily lowering the temperature to a steady-sate doneness. This means that it can be possible to control the unknown states to achieve the perfect cooking result.

The main conclusion of this work is that it is possible to use control theory and mathematical modelling to get idealized roasted meat. The results suggest that the model-based roasting control is a promising alternative to use intuition, fingertip methods, guessing and speculation to get even temperature distribution for a roast. Future study of this approach is recommended.

# Bibliography


[1] Harold McGee. *On food and cooking: the science and lore of the kitchen*. Simon and Schuster, 2007.

[2] S Joe Qin and Thomas A Badgwell. "A survey of industrial model predictive control technology." In: *Control engineering practice* 11.7 (2003), pp. 733–764.

[3] C Aurora et al. "Predictive control of thermal power plants." In: *International Journal of Robust and Nonlinear Control: IFAC-Affiliated Journal* 14.4 (2004), pp. 415–433.

[4] Gohar Gholamibozanjani et al. "Model predictive control strategy applied to different types of building for space heating." In: *Applied energy* 231 (2018), pp. 959–971.

[5] Monika Bakošová and Juraj Oravec. "Robust model predictive control for heat exchanger network." In: *Applied Thermal Engineering* 73.1 (2014), pp. 924–930.

[6] Liuping Wang, Stephen Smith, and Charlie Chessari. "Continuous-time model predictive control of food extruder." In: *Control Engineering Practice* 16.10 (2008), pp. 1173–1183.

[7] Timothy A Haley and Steven J Mulvaney. "On-line system identification and control design of an extrusion cooking process: Part II. Model predictive and inferential control design." In: *Food control* 11.2 (2000), pp. 121–129.

[8] Sutanto Hadisupadmo, Edi Leksono, et al. "Model predictive control design and performance analysis of a pasteurization process plant." In: *2016 International Conference on Instrumentation, Control and Automation (ICA)*. IEEE. 2016, pp. 81–87.

[9] Tobias Gybel Hovgaard et al. "Model predictive control technologies for efficient and flexible power consumption in refrigeration systems." In: *Energy* 44.1 (2012), pp. 105–116.

[10] *FAO's Animal Production and Health Division: Meat & Meat Products*. `http://www.fao.org/ag/againfo/themes/en/meat/backgr_composition.html`. (Accessed on 05/08/2021).

[11] Larry Meadows. *Blog Archives Category: food and nutrition | USDA*. `https://www.usda.gov/media/blog/archive/category/food-and-nutrition`. (Accessed on 05/08/2021). Sept. 2019.

[12] United States. "Institutional meat purchase specifications for fresh beef products." English. In: (1996), USDA. URL: `http://handle.nal.usda.gov/10113/38279`.

[13] Nortura bondens selskap. *Norsk Kjøttfe - Medlemsportal for Nortura SA*. https://medlem.nortura.no/storfe/norsk-kjoettfe/. (Accessed on 05/08/2021).

[14] Howard J Swatland. *Structure and development of meat animals and poultry*. CRC Press, 1994.

[15] Nordic Council of Ministers Nordic Council of Ministers. "Nordic Nutrition Recommendations 2012." In: *Nordic Nutrition Recommendations 2012* 5.11 (Aug. 2008), pp. 1–3. DOI: 10.6027/nord2014-002. URL: https://doi.org/10.6027/nord2014-002.

[16] Rabia Shabir Ahmad, Ali Imran, and Muhammad Bilal Hussain. "Nutritional composition of meat." In: *Meat science and nutrition* 4 (2018).

[17] Klaus G. Grunert, Lone Bredahl, and Karen Brunsø. "Consumer perception of meat quality and implications for product development in the meat sector—a review." In: *Meat Science* 66.2 (2004), pp. 259–272. DOI: https://doi.org/10.1016/S0309-1740(03)00130-X. URL: https://www.sciencedirect.com/science/article/pii/S030917400300130X.

[18] Mohammed Gagaoua et al. "Inter-laboratory assessment by trained panelists from France and the United Kingdom of beef cooked at two different end-point temperatures." In: *Meat Science* 122 (2016), pp. 90–96. DOI: https://doi.org/10.1016/j.meatsci.2016.07.026. URL: https://www.sciencedirect.com/science/article/pii/S0309174016302455.

[19] J.J. HARRIS et al. "Evaluation of the Tenderness of Beef Top Sirloin Steaks." In: *Journal of Food Science* 57.1 (1992), pp. 6–9. DOI: https://doi.org/10.1111/j.1365-2621.1992.tb05412.x. eprint: https://onlinelibrary.wiley.com/doi/pdf/10.1111/j.1365-2621.1992.tb05412.x. URL: https://onlinelibrary.wiley.com/doi/abs/10.1111/j.1365-2621.1992.tb05412.x.

[20] R. L. Hostetler et al. "Influence of Carcass Position During Rigor Mortis on Tenderness of Beef Muscles: Comparison of two Treatments." In: *Journal of Animal Science* 31.1 (July 1970), pp. 47–50. DOI: 10.2527/jas1970.31147x. eprint: https://academic.oup.com/jas/article-pdf/31/1/47/23200278/jan0310010047.pdf. URL: https://doi.org/10.2527/jas1970.31147x.

[21] P. E. BOUTON et al. "A comparison of the effects of some post-slaughter treatments on the tenderness of beef." In: *International Journal of Food Science & Technology* 8.1 (1973), pp. 39–49. DOI: https://doi.org/10.1111/j.1365-2621.1973.tb01687.x. eprint: https://ifst.onlinelibrary.wiley.com/doi/pdf/10.1111/j.1365-2621.1973.tb01687.x. URL: https://ifst.onlinelibrary.wiley.com/doi/abs/10.1111/j.1365-2621.1973.tb01687.x.

[22] E Obuz, ME Dikeman, and TM Loughin. "Effects of cooking method, reheating, holding time, and holding temperature on beef longissimus lumborum and biceps femoris tenderness." In: *Meat Science* 65.2 (2003), pp. 841–851.

[23] Pankaj B Pathare and Anthony Paul Roskilly. "Quality and energy evaluation in meat cooking." In: *Food Engineering Reviews* 8.4 (2016), pp. 435–447.

[24] Grethe Andersen and Camilla Bejerholm2and Ina Clausen. "Effect of resting time on sensory quality and loss of meat juice in pork, beef and veal." In: *International Congress of meat Science and Technology, 25-30 august 2002, Rome, Italy*. 2002.

[25] EVA Tornberg. "Effects of heat on meat proteins–Implications on structure and quality of meat products." In: *Meat science* 70.3 (2005), pp. 493–508.

[26] Ina Clausen and Lars Ovesen. "Changes in fat content of pork and beef after pan-frying under different conditions." In: *Journal of Food Composition and Analysis* 18.2 (2005), pp. 201–211. DOI: https://doi.org/10.1016/j.jfca.2004.03.024. URL: https://www.sciencedirect.com/science/article/pii/S0889157504000638.

[27] Krystyna Palka and Henryk Daun. "Changes in texture, cooking losses, and myofibrillar structure of bovine M. semitendinosus during heating." In: *Meat science* 51.3 (1999), pp. 237–243.

[28] RY Murphy et al. "Heat transfer properties, moisture loss, product yield, and soluble proteins in chicken breast patties during air convection cooking." In: *Poultry Science* 80.4 (2001), pp. 508–514.

[29] Jorge Mir-Bel, Rosa Oria, and Marıéa L Salvador. "Influence of temperature on heat transfer coefficient during moderate vacuum deep-fat frying." In: *Journal of Food Engineering* 113.2 (2012), pp. 167–176.

[30] Sergio R Vaudagna et al. "Sous vide cooked beef muscles: effects of low temperature–long time (LT–LT) treatments on their quality characteristics and storage stability." In: *International journal of food science & technology* 37.4 (2002), pp. 425–441.

[31] *Kommunehelsa*. http://khs.fhi.no/webview/. (Accessed on 05/04/2021).

[32] R Vikse et al. "Heterocyclic amines in cooked meat." In: *Tidsskrift for den Norske laegeforening: tidsskrift for praktisk medicin, ny raekke* 119.1 (1999), pp. 45–49.

[33] Victor W Zhong et al. "Protein foods from animal sources, incident cardiovascular disease and all-cause mortality: a substitution analysis." In: *International Journal of Epidemiology* (2021).

[34] *List of Classifications – IARC Monographs on the Identification of Carcinogenic Hazards to Humans*. https://monographs.iarc.who.int/list-of-classifications. (Accessed on 05/04/2021).

[35] Solveig Langsrud et al. "Cooking chicken at home: Common or recommended approaches to judge doneness may not assure sufficient inactivation of pathogens." In: *PLOS ONE* 15.4 (2020), e0230928. DOI: 10.1371/journal.pone.0230928.

[36] Benjamin Caballero, Luiz C Trugo, and Paul M Finglas. *Encyclopedia of food sciences and nutrition*. Academic, 2003.

[37] Michèle Marcotte, Ali R. Taherian, and Yousef Karimi. "Thermophysical properties of processed meat and poultry products." In: *Journal of Food Engineering* 88.3 (2008), pp. 315–322. DOI: https://doi.org/10.1016/

j.jfoodeng.2008.02.016. URL: https://www.sciencedirect.com/science/article/pii/S0260877408000940.

[38] Refrigerating American Society of Heating and Air-Conditioning Engineers. *2006 ASHRAE Handbook: Refrigeration*. ASHRAE Handbook Refrigeration SI. American Society of Heating, Refrigeration and Air-Conditioning Engineers, 2006, pp. 9.1–9.28. URL: https://books.google.no/books?id=touHPwAACAAJ.

[39] Jérémie Cernela, Bertrand Heyd, and Bertrand Broyart. "Evaluation of heating performances and associated variability of domestic cooking appliances (oven-baking and pan-frying)." In: *Applied thermal engineering* 62.2 (2014), pp. 758–765.

[40] Alain Kondjoyan et al. "Combined heat transfer and kinetic models to predict cooking loss during heat treatment of beef meat." In: *Meat science* 95.2 (2013), pp. 336–344.

[41] Heli Chen and Bernie D Shizgal. "A spectral solution of the Sturm–Liouville equation: comparison of classical and nonclassical basis sets." In: *Journal of computational and applied mathematics* 136.1-2 (2001), pp. 17–35.

[42] Bjarne Foss and Tor Aksel N Heirung. "Merging optimization and control." In: *Lecture Notes* (2013).

[43] David Q Mayne et al. "Constrained model predictive control: Stability and optimality." In: *Automatica* 36.6 (2000), pp. 789–814.

[44] James B Rawlings. "Tutorial overview of model predictive control." In: *IEEE control systems magazine* 20.3 (2000), pp. 38–52.

[45] "Effect of Model Plant Mismatch on MPC Performance and Mismatch Threshold Determination." In: *Procedia Engineering* 148 (2016). Proceeding of 4th International Conference on Process Engineering and Advanced Materials (ICPEAM 2016), pp. 1008–1014. DOI: https://doi.org/10.1016/j.proeng.2016.06.518. URL: https://www.sciencedirect.com/science/article/pii/S1877705816309857.

[46] N. Lawrence Ricker Alberto Bemporad and Manfred Morari. *Model Predictive Control Toolbox™ Reference*. (Accessed on 05/06/2021). 2021. URL: https://www.mathworks.com/help/pdf_doc/mpc/mpc_ref.pdf.

[47] Theodore L Bergman et al. *Fundamentals of heat and mass transfer*. John Wiley & Sons, 2011.

[48] John Harrison. "Fast and accurate Bessel function computation." In: *2009 19th IEEE Symposium on Computer Arithmetic*. IEEE. 2009, pp. 104–113.

[49] *MEATER® | Wireless Smart Meat Thermometer | For BBQ & Kitchen Cooking*. https://meater.com/. (Accessed on 05/13/2021).

[50] *MEATER Customer Support*. https://support.meater.com/faqs/internal-temperature-meater. (Accessed on 05/13/2021).

[51] *MEATER+ Specification – MEATER US*. https://store-us.meater.com/pages/meater-specification-1. (Accessed on 05/13/2021).

[52] *Bosch serie-8 oven HMG8764.6*. https://media3.bosch-home.com/Documents/9001283299_B.pdf. (Accessed on 05/19/2021).

# A | Numerical Computation of the Eigenvalues

## A.1 The Spectral method for the 1-d Heat Equation

Let $z = L\omega$, so that the roots of the eigenvalues may be found for a non-polynomial equation, viz.

$$f(z) = z \tan\left(\frac{z}{2}\right) - \mathrm{Bi} = 0 \tag{A.1}$$

It can be problematic with a unbounded tangent trigonometric at regular intervals. Multiplying both sides of the equation with $cos(z/2)$ yields a relation with better behavior.

$$g(z) = z \sin\left(\frac{z}{2}\right) - \mathrm{Bi} \cos\left(\frac{z}{2}\right) = 0 \tag{A.2}$$

Newton's method are used for the numerics. We can Observe that

$$g'(z) = \left(1 + \frac{\mathrm{Bi}}{2}\right) \sin\left(\frac{z}{2}\right) + \frac{z}{2} \cos\left(\frac{z}{2}\right) \tag{A.3}$$

Let $z_0$ denote an initial guess for $z$. For an initial guesses of $tan(z/2)$, i.e.

$$2\pi n, \quad n \in \mathbb{N} \tag{A.4}$$

successive guesses are obtained via the iteration

$$z_{k+1} = z_k - \frac{f\left(z_k\right)}{f'\left(z_{k+1}\right)} = z_k - \frac{z_k \sin\left(\frac{z_k}{2}\right) - \mathrm{Bi} \cos\left(\frac{z_k}{2}\right)}{\left(1 + \frac{\mathrm{Bi}}{2}\right) \sin\left(\frac{z_k}{2}\right) + \frac{z_k}{2} \cos\left(\frac{z_k}{2}\right)} \tag{A.5}$$

## A.2 The Spectral method for the 2-d Heat Equation

We recover the Robin boundary condition and the eigenvalues of $g(\lambda)$ can be found via Newtons methods.

$$g(\lambda) = L_c \lambda J_1(\lambda a) + \mathrm{Bi}\, J_0(\lambda a) = 0 \tag{A.6}$$

The derivative of $g(\lambda)$ becomes.

$$g(\lambda)' = L_c a \lambda J_0(\lambda a) - \mathrm{Bi}\, a J_1(\lambda a) \tag{A.7}$$

The eigenvalues can be found via iteration, with an initial guess of $\lambda_0 = \sqrt{\frac{2}{\pi}} \cos(\pi/4)$

$$\lambda_{k+1} = \lambda_k - \frac{f(\lambda_k)}{f'(\lambda_k)} = \lambda_k - \frac{L_c \lambda J_1(\lambda a) + \mathrm{Bi}\, J_0(\lambda a)}{L_c a \lambda J_0(\lambda a) - \mathrm{Bi}\, a J_1(\lambda a)} \tag{A.8}$$

# B | Check of Orthogonality

## B.1 The Spectral method for the 1-d Heat Equation

```
clc;clear all; close all;

Bi = 20; % Constant
n = 20; % Modes
L = 1; % Length

%% Find roots
it = 2*pi*(0:n)+2; % Itertation domian

lam = zeros(1,n-1); % Pre Allocate

for i = 1:length(it)

    problem.objective   = @(omega) L*omega*sin((L*omega)
       /2) - Bi*cos((L*omega)/2);
    problem.x0          = it(i);
    problem.solver      = 'fzero';
    problem.options     = optimset(@fzero);

    lam(i) = fzero(problem);
    if lam(i) <= 0
        lam(i) = [];
    end
    lam(lam == 0) = [];
    lam(isnan(lam)) = [];

end

lam = uniquetol(lam)./L;
omg = lam(1:n);


```

```
32 %% Orthogonality
33
34 wi = omg'*ones(1,length(omg));
35 wj = ones(length(omg),1)*omg;
36
37 f = @(x) cos((x-(L/2)).*wi).*cos((x-(L/2)).*wj);
38 checkorth = integral(f,0,L,'ArrayValued',true);
39
40 %% Plot Orthogonality
41 figure
42 imagesc(checkorth)
```

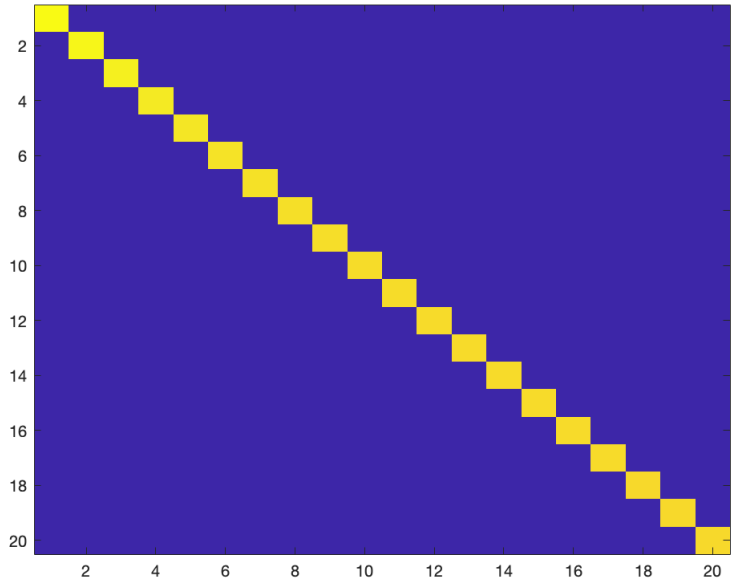


Figure B.1: An image that displays scaled colours to verify that the spectral method for the SLP is orthogonal with 20 modes. The blue colour is approximately zeros and yellow are non zero values.

## B.2 Orthogonality for the 2-D spectral Method

Let $R_n(r)$ and $R_m(r)$ satisfy the Sturm Liouville problem. Subject to the Robin boundary condition, viz.

$$R_m \frac{d}{dr}\left(r\frac{dR_n}{dr}\right) - R_n \frac{d}{dr}\left(r\frac{dR_m}{dr}\right) + (\lambda_n - \lambda_m)\, r R_n R_m = 0 \tag{B.1}$$

We perceive with integrating from 0 to $a$.

$$\int_0^a \left(R_m \frac{d}{dr}\left(r\frac{dR_n}{dr}\right) - R_n \frac{d}{dr}\left(r\frac{dR_m}{dr}\right)\right) dr + (\lambda_n - \lambda_m) \int_0^a r R_n R_m dr = 0 \tag{B.2}$$

We will consider the first part of the integrand and use integration by parts with the BC. Verify that

$$\begin{aligned} \int_0^a R_m \frac{d}{dr}\left(r\frac{dR_n}{dr}\right) dr &= \left[r R_m \frac{dR_n}{dr}\right]_0^a - \int_0^a r \frac{dR_n}{dr}\frac{dR_m}{dr} dr \\ &= \left[a \frac{dR_m}{dr}\frac{L_c}{\mathrm{Bi}}\frac{dR_n}{dr}\right]_0^a - \int_0^a r \frac{dR_n}{dr}\frac{dR_m}{dr} dr \end{aligned} \tag{B.3}$$

Likewise for the second part of the integral

$$\begin{aligned} \int_0^a R_n \frac{d}{dr}\left(r\frac{dR_m}{dr}\right) dr &= \left[r R_n \frac{dR_m}{dr}\right]_0^a - \int_0^a r \frac{dR_m}{dr}\frac{dR_n}{dr} dr \\ &= \left[a \frac{dR_m}{dr}\frac{L_c}{\mathrm{Bi}}\frac{dR_m}{dr}\right]_0^a - \int_0^a r \frac{dR_m}{dr}\frac{dR_n}{dr} dr \end{aligned} \tag{B.4}$$

Insert the equations back, yields a orthogonality relationship.

$$(\lambda_n - \lambda_m) \int_0^a r R_n R_m dr = 0 \Rightarrow \int_0^a r R_n R_m dr = 0 \quad \text{if} \quad n \neq m \tag{B.5}$$

The orthogonality condition for the Bessel functions becomes

$$\int_0^a r J_0\left(\Gamma_n \frac{r}{a}\right) J_0\left(\Gamma_m \frac{r}{a}\right) dr = 0 \quad \text{if} \quad n \neq m \tag{B.6}$$

## B.3 Orthogonality Check for the 2-D Spectral Method

```
%% Coefficients
Bi = 20; % Constant
n = 20; % Modes
r = 1; % Length

%% Find Roots
it = 0:0.1:n*3.3;  % Itertation domian
lam = zeros(1,n);  % Pre Allocate


for i = 1:length(it)

    problem.objective   = @(gamma) -gamma*besselj(1,
       gamma) + Bi*besselj(0,gamma);
    problem.x0          = it(i);
    problem.solver      = 'fzero';
    problem.options     = optimset(@fzero);

    lam(i) = fzero(problem);
    if lam(i) <= 0
        lam(i) = [];
    end
    lam(lam == 0) = [];
    lam(isnan(lam)) = [];

end

lam = uniquetol(lam);

w = lam(1:n);
Lambdda = w./r;

%% Check Orthogonal
wi = w'*ones(1,length(w));
wj = ones(length(w),1)*w;
a = r;

Fi = @(R) R.*besselj(0,wi.*R/a).*besselj(0,wj.*R/a);
checkorth = integral(Fi,0,a,'ArrayValued',true);
figure
imagesc(checkorth)
```

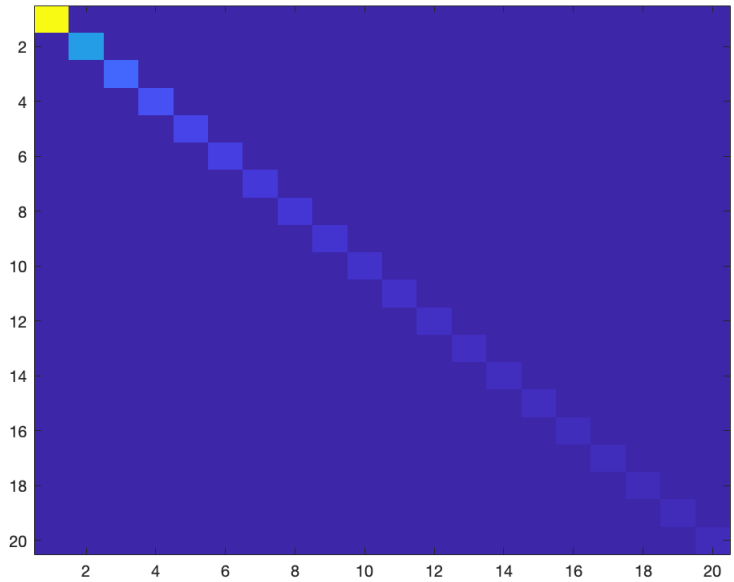


Figure B.2: An image that displays scaled colours to verify that the spectral method for the SLP is orthogonal with 20 modes. The blue colour is approximately zeros, and the other colours are non zero values.

# C | Result

## C.1 Telemetry for the Tenderloin

| Time [min] | Probe 1 | Probe 2 | Probe 3 | u ovn | u probe 1 | u probe 2 |
|---|---|---|---|---|---|---|
| 0 | 17 | 17 | NaN | 250 | 40 | 40 |
| 2 | 17 | 18 | 19 | 250 | 150 | 162 |
| 4 | 17 | 18 | 20 | 250 | 172 | 187 |
| 6 | 17 | 19 | 21 | 250 | 190 | 209 |
| 8 | 18 | 21 | 22 | 250 | 195 | 216 |
| 10 | 19 | 25 | 24 | 250 | 195 | 218 |
| 12 | 20 | 28 | 25 | 250 | 198 | 220 |
| 14 | 22 | 32 | 27 | 250 | 220 | 237 |
| 16 | 24 | 36 | 30 | 250 | 229 | 241 |
| 18 | 26 | 39 | 32 | 250 | 228 | 241 |
| 20 | 29 | 43 | 35 | 250 | 227 | 242 |
| 22 | 32 | 47 | 38 | 250 | 227 | 239 |
| 24 | 35 | 51 | 41 | 250 | 223 | 237 |
| 26 | 38 | 54 | NaN | 25 | 145 | 160 |
| 28 | 41 | 57 | NaN | 25 | 86 | 98 |
| 30 | 44 | 59 | NaN | 25 | 59 | 64 |
| 32 | 47 | 59 | NaN | 25 | NaN | NaN |
| 34 | 49 | 60 | NaN | 25 | NaN | NaN |
| 36 | 51 | 59 | NaN | 25 | NaN | NaN |
| 38 | 53 | 59 | NaN | 25 | NaN | NaN |
| 40 | 54 | 58 | NaN | 25 | NaN | NaN |
| 42 | 55 | 57 | NaN | 25 | NaN | NaN |
| 44 | 55 | 56 | NaN | 25 | NaN | NaN |
| 46 | 55 | 55 | NaN | 25 | NaN | NaN |

## C.2 Telemetry for the Round Steak

| Time [min] | Probe 1 | Probe 2 | Probe 3 | u oven | u probe 1 | u probe 2 |
|---|---|---|---|---|---|---|
| 0 | 7 | 8 | 8 | 250 | NaN | NaN |
| 2 | 7 | 8 | 8 | 250 | NaN | NaN |
| 4 | 7 | 9 | 8 | 250 | NaN | NaN |
| 6 | 7 | 11 | 10 | 250 | NaN | NaN |
| 8 | 7 | 14 | 13 | 250 | NaN | NaN |
| 10 | 8 | 17 | 16 | 250 | NaN | NaN |
| 12 | 8 | 20 | 19 | 250 | 215 | 202 |
| 14 | 9 | 24 | 21 | 250 | 215 | 203 |
| 16 | 10 | 27 | 25 | 250 | 215 | 203 |
| 18 | 12 | 31 | 27 | 250 | 213 | 203 |
| 20 | 14 | 34 | 30 | 250 | 212 | 203 |
| 22 | 15 | 37 | 32 | 250 | 211 | 202 |
| 24 | 17 | 40 | 35 | 250 | 210 | 202 |
| 26 | 19 | 42 | 36 | 250 | 209 | 202 |
| 28 | 22 | 45 | 39 | 250 | 209 | 202 |
| 30 | 24 | 47 | 42 | 250 | 209 | 202 |
| 32 | 27 | 50 | 44 | 250 | 208 | 203 |
| 34 | 29 | 52 | NaN | 25 | 130 | 128 |
| 36 | 31 | 54 | NaN | 25 | 75 | 77 |
| 38 | 34 | 55 | NaN | 25 | 53 | NaN |
| 40 | 36 | 55 | NaN | 25 | NaN | NaN |
| 42 | 39 | 54 | NaN | 25 | NaN | NaN |
| 44 | 41 | 54 | NaN | 25 | NaN | NaN |
| 46 | 42 | 53 | NaN | 25 | NaN | NaN |
| 48 | 44 | 52 | NaN | 25 | NaN | NaN |
| 50 | 45 | 51 | NaN | 25 | NaN | NaN |
| 52 | 46 | 50 | NaN | 25 | NaN | NaN |
| 54 | 47 | 49 | NaN | 25 | NaN | NaN |
| 56 | 47 | 48 | NaN | 25 | NaN | NaN |
| 58 | 48 | 47 | NaN | 25 | NaN | NaN |
| 60 | 48 | 47 | NaN | 25 | NaN | NaN |

Eystein Gulbrandsen

# Model-Based Roasting Control

NTNU
Kunnskap for en bedre verden